POLITECNICO DI MILANO
School of Industrial and Information Engineering
Master of Science in Computer Science & Engineering
Department of Electronics, Information and Bioengineering

STUDY OF HUNTINGTON'S DISEASE THROUGH CORTICAL THICKNESS ANALYSIS

Politecnico di Milano

Supervisor: Prof. Giacomo Boracchi
Co-Supervisor: Dott. Simone Melzi

Author:
Andrea Filippozzi, matricola 894582

Academic Year 2019-2020

Ai miei genitori

Contents

List of Figures

List of Tables

Sommario

La malattia di Huntington è una malattia neurodegenerativa genetica e autosomica dominante che colpisce la mobilità muscolare e porta inevitabilmente a degenerazione cognitiva e problemi psichiatrici. Uno dei sintomi della malattia di Huntington è la morte di alcuni neuroni nel cervello e la conseguente atrofia dell'organo cerebrale. Per atrofia cerebrale si intende la riduzione del tessuto cerebrale, conseguente alla necrosi e al restringimento delle cellule che compongono il suddetto tessuto. L'atrofia cerebrale comporta una perdita delle funzioni svolte dal cervello. L'entità di questa perdita dipende dall'estensione delle aree cerebrali interessate dai processi di necrosi e restringimento cellulare.
Poiché la malattia di Hungtington è una malattia genetica, esistono test genetici utili per identificare e diagnosticare la predisposizione all'insorgenza della malattia. Non esiste ancora una cura per la malattia di Huntington e l'unico intervento medico possibile è la prescrizione di farmaci in grado di rallentare e arginare i sintomi sia fisici che psichiatrici. Prima viene trattato un paziente, più efficace sarà il trattamento e potrà posticipare l'insorgenza dei sintomi.
Per capire se un trattamento è efficace e può cambiare il decorso naturale della malattia, dobbiamo misurare e prevedere la progressione della malattia. Purtroppo la medicina non è ancora in grado di identificare i gradi di sviluppo della malattia di Huntington, in particolare durante le prime fasi, quelle presintomatiche, in cui i cambiamenti sono più sottili e difficili da percepire. Un metodo per studiare e prevedere la malattia di Huntington si basa sull'analisi della risonanza magnetica per immagini (MRI). Una scansione MRI è un metodo non invasivo e invivo, in grado di misurare il volume e lo spessore delle strutture cerebrali. Molti studi sono stati condotti con l'utilizzo di questa tecnologia e hanno dimostrato come diverse aree del tessuto cerebrale siano interessate dalla malattia di Huntington, provocandone la diminuzione di volume e il conseguente assottigliamento.
L'obiettivo della tesi è trovare un algoritmo in grado di distinguere i controlli sani dai pazienti presintomatici. L'ipotesi di partenza è che la struttura delle superfici cerebrali, in particolare lo spessore del tessuto cerebrale, sia interessata dalla degenerazione della malattia di

Huntington. Attraverso l'applicazione di due diversi metodi, il primo più generale, il secondo più specifico, che utilizza un algoritmo di shape matching per ottenere una registrazione specifica dell'utente dei cervelli analizzati, l'obiettivo è quello di riuscire a distinguere i controlli sani dai pazienti con malattia di Huntington attraverso un'analisi effettuata sulla diminuzione dello spessore, che può evidenziare una netta linea di separazione tra le due categorie analizzate.

Abstract

Huntington's disease is a genetic and autosomal dominant neurodegenerative disease that affects muscle mobility and inevitably leads to cognitive degeneration and psychiatric problems. One of the symptoms of Huntington's disease is the death of some neurons in the brain and the consequent atrophy of the brain organ. By cerebral atrophy we mean the reduction of the brain tissue, resulting from the necrosis and shrinking of the cells that make up the aforementioned tissue. Brain atrophy involves a loss of the functions performed by the brain. The extent of this loss depends on the extent of the brain areas affected by the processes of cellular necrosis and shrinkage.
Since Hungtington's disease is a genetic disease, there are genetic tests that are useful for identifying and diagnosing the predisposition to the onset of the disease. There is still no cure for Huntington's disease and the only possible medical intervention is the prescription of medicines that can slow down and stem both physical and psychiatric symptoms. The sooner a patient is treated, the more effective the treatment will be and will be able to postpone the onset of symptoms.
To understand if a treatment is effective and can change the natural course of the disease, we need to measure and predict the progression of the disease. Unfortunately, medicine is still unable to identify the degrees of development of Huntington's disease, particularly during the early stages, the presymptomatic ones, in which the changes are more subtle and difficult to perceive. A method to study and predict Huntington disease is based on the analysis of Magnetic Resonance Imaging (MRI). An MRI scan is a non-invasive and invivo method, that can measure the volume and thickness of brain structures. Many studies have been done with the use of this technology and have shown how different areas of the brain tissue are affected by Huntington's disease, causing the decreasing in volume and consequent thinning.
The goal of the thesis is to find an algorithm to distinguish healthy controls from presymptomatic patients. The starting hypothesis is that the structure of the brain surfaces, in particular the thickness of the brain tissue, is affected by the degeneration of the Huntington's disease. Through the application of two different methods, the former more

general, the latter more specific, that uses a shape matching algorithm to obtain a user-specific registration of the analyzed brains, the goal is to be able to distinguish healthy controls from patients with Huntington's disease through an analysis carried out on the decrease in thickness, that can highlight a clear separating line between the two categories analyzed.

Ringraziamenti

Ringrazio tutti coloro che mi hanno accompagnato, sostenuto, spronato e allietato durante questo mio percorso di laurea magistrale. Senza di voi questo cammino sarebbe stato molto più tortuoso e non avrei potuto vivere a pieno tutte le esperienze che hanno caratterizzato questa parte della mia vita.

In primis, ringrazio la mia famiglia che è sempre stata al mio fianco, sia nei momenti migliori, sia in quelli così difficili da sembrare insormontabili.
Ringrazio mia mamma Elena che mi ha sempre incoraggiato a impegnarmi al massimo, mi ha spronato a non mollare mai e che è sempre stata al mio fianco con amore.
Ringrazio mio papà Marco che non è mai stato pressante e opprimente, che mi ha sempre lasciato libero di fare quello che desideravo, ma che si è sempre interessato a quello che facevo sostenendomi in tutto il percorso.
Ringrazio mio fratello Enrico per le partitelle al campetto di basket, per le serate e per gli allenamenti insieme, per i momenti passati davanti a qualche gioco da tavolo che mi hanno permesso di divertirmi e di rilassarmi.

Ringrazio Marta che mi ha sempre sostenuto e incoraggiato, che è sempre stata orgogliosa di me e con la quale ho vissuto giornate indimenticabili; per aver reso ogni singolo momento trascorso insieme intenso e speciale; per avermi amato nei momenti felici e per averlo fatto ancora più intensamente in quelli di scorforto e debolezza. La ringrazio perchè c'è sempre stata e sempre ci sarà.

Ringrazio i miei compagni e fratelli di università Edo, Ciccio e Frys, con i quali ho trascorso le mie giornate meneghine tra università, Well Done e casa di Ciccio, per prepararsi agli esami. Grazie a voi che avete reso questo percorso più piacevole e che mi avete fatto trascorrere momenti spassosi e divertenti giorno per giorno.
In particolare vorrei dedicare un ringraziamento speciale a Edo, coinquilino in questi ultimi anni, che ha reso tutte le giornate più leggere e

gioiose e che ha sopportato tutti i miei difetti.

Ringrazio i miei amici di una vita con i quali ho trascorso sempre weekend gioviali e rilassanti e che sono sempre stati presenti quando ne ho avuto bisogno.

Ringrazio infine, ma non per ultimi, il mio relatore Giacomo Boracchi e il mio correlatore Simone Melzi per il loro prezioso aiuto e per le direttive durante il lavoro.

Chapter 1

Introduction

Huntington's disease is an inherited disease caused by the degeneration of brain cells located in specific areas of the brain. It is characterized by a more frequent onset in adulthood but can in fact arise at any age, from infancy to old age. The brain cells affected by the degenerative process are found in deep structures of the brain but also the cells of the outer part of the brain (cerebral cortex) which are essential to functions such as thinking, perception and memory are involved in varying degrees. The characteristic clinical picture that derives from the progressive degeneration of neurons in the indicated areas includes both involuntary movements and a reduction in cognitive abilities and mood alterations. As things currently stand, there are still no medicines capable of curing the disease or interrupting its course. The neurologist can prescribe various drug therapies to control the main motor and/or psychiatric symptoms that characterize Huntington's disease, but these medicines are only useful for relieving the symptoms and improving the patient's quality of life. However, it is essential to start therapy as soon as possible to make the treatment more effective and to guarantee the patient a greater quality and longevity of life. The crucial problem is the fact that it is difficult to identify a Huntington's patient, especially at the presymptomatic stage; therefore it becomes important to find an effective method that succeeds in this purpose.
The goal of the thesis is to find an algorithm able to divide healthy patients from presymptmatic ones. The starting hypothesis is that the structure of the brain surfaces, in particular the thickness of the brain tissue, is affected by Huntington's disease. I will present two methods that use cortical thickness analysis to highlight the presence or absence of a separation between healthy and sick patients. The former, more general, will have as a starting point a global registration of the patients' brains, while the latter, more specific, will use a user-specific registration using the Functional maps algorithm.
The analyzes were performed on a cross-sectional and longitudinal MRI

brain scan dataset, provided by IBM and from the CHDI foundation, which included 41 early HD patients (4 visits each one) and 44 healthy controls (7 visits each one).
The contents of the thesis will be structured in this way. First of all, in chapter 2, the background of the thesis will be analyzed in detail. In particular, an overview of Huntington's disease, its history, etiology and the resulting symptoms will be presented, both at the macroscopic and at the microscopic level. The chapter will continue with the physical explanation of how MRI brain imaging occurs, followed by how these images are digitally processed through software called Freesurfer. The chapter will end by illustrating a particular shape matching technique, Functional Maps which I used for my analysis of Huntington's disease. This approach, used within the thesis, considers the mappings between functions defined on the shapes, rather than correspondence of points on the shapes. I have chosen Functional maps because this method is able to create a map between two brains of the same patient but at different time instant. This allows to obtain a user-specific registration of the brain, which may have more precise information than a global record of brains: in particular, it is possible to have a map that allows to better compare the cortical thickness of patients in order to identify Huntington's disease.
Chapter 3 is a detailed description of how the problem was approached, illustrating the two methods proposed one after the other.
Chapter 4 will contain an explanation of the data available, on which I carried out my tests and in the next chapter (chapter 5) the results obtained by the proposed methods will be shown. The results show that cortical thickness degeneration is evident in sick patients, even in a presymptomatic state and are validated by the use of two statistical tests: the Kruskal-Wallis test and the Wilcoxon Rank Sum test which confirm the initial hypothesis and which therefore makes it possible to distinguish a Huntington's patient even before the first symptoms appear. This result can make it possible to act more promptly, anticipating the start of drug therapy and therefore increasing the chances of its benefit.
Finally, chapter 6 contains the conclusions of the work done and the comparison between the two method used showing the effectiveness or otherwise of the methods and the advantages of using one over the other.

Chapter 2

Background

In this chapter I intend to explain in what context my thesis work is placed. In particular, in the first part an overview of Huntinton's disease will be presented, illustrating its history, spread, etiology and pathogenesis. The second section will show how MRI images are extracted and how they are reprocessed using a digital processing software, Freesurfer. In the final section, on the other hand, a shape matching method is presented, Functional Maps, which will then be used in one of the two methods proposed in my work.

2.1 Huntington Desease

Huntington's disease, or Huntington's chorea (pronounced: chorea or chorea), is a genetic neurodegenerative disease that affects muscle mobility and inevitably leads to cognitive degeneration and psychiatric problems. The first symptoms typically appear during adulthood and more frequently during middle age; it is the most frequent disease due to genetics which has involuntary movements of the locomotor system as symptoms (which are called chorea). The worldwide prevalence of Huntington's disease is 5-10 cases per 100,000 people, but it varies widely due to ethnicity and migration. People of Western European descent have such a genetic predisposition that Huntington's disease is more common, with an average of around 3-7 cases per 100,000 people, than those of Asian or African descent in which the incidence rate is around 1 in 1,000,000 [1].
The disease is caused by an autosomal dominant mutation in one of two copies (alleles) of a gene encoding a protein called huntingtin, which means that the independent probability of inheriting the disease from a person with the disease for each child is 50%. Physical symptoms of the disease can begin to manifest even at a young age, but more frequently between the ages of 35 and 44.
The disease does not manifest itself with the same symptoms even

among individuals with the disease of the same family, but usually the progression of symptoms can be broadly predicted. The first manifestations are often mild mood or cognitive problems resulting in a lack of general coordination and motor instability. As the disease progresses, the unstable coordination of the body becomes increasingly evident and is accompanied by a progressive worsening of mental abilities and the appearance of behavioural and psychiatric problems.
Life expectancy at the onset of the first symptoms is around 20 years due to possible complications, such as pneumonia, physical damage from falls and heart disease, given by the weakness of the body. There is still no cure for Huntington's disease and full-time care in the more advanced stages of the disease becomes indispensable. There are no surgical treatments, so the only applicable treatments are the pharmacological ones that try to alleviate its many symptoms, even if not by much.

2.1.1 History of Huntington's disease

The cause of Huntington's disease remained unknown until the last decades of the twentieth century, although Huntington's chorea had been recognized and cataloged as a disorder since the Middle Ages. Originally it was simply called "chorea", a word of Greek origin whose literal meaning is "dance in unison", due to the typical jerky dancing movements; later it was also renamed "hereditary chorea" and "chronic progressive chorea" due to its condition of inheritance and progressive degeneration.
The first complete description of the disease was by George Huntington, from whom it later took its name, and was in 1872 [2]. He was able to understand by examining the medical history of several generations of a family who had very similar symptoms, which these conditions had to be somehow related. Even in Europe, the disease aroused great interest among scientists, including Louis Theophile Joseph Landouzy, Camillo Golgi, Desire-Magloire Bourneville and Joseph Jules Dejerine, so much so that at the end of the 19th century the greatest amount of data and results on the disease was European.
By the late 1900s, the disease was now known around the world as a condition in its own right. An important breakthrough in Huntington's disease research came in 1983 with the discovery of the approximate location of a causal gene. In 1993 was isolated the specific gene responsible of the disease [3].

2.1.2 Etiology of Huntington's disease

Huntington's disease is caused by abnormal stretching of a specific section of a gene repeatedly. This gene is the HTT gene which is located on

the short arm of chromosome 4. The HTT gene consists of a three-base sequence of DNA: cytosine-adenine-guanine (CAG), repeated several times in a succession, known as expansion of a hat-trick. For this reason, Huntington's disease is classified as one of the triplet expansion diseases [4]. A healthy person has fewer than 36 CAG repeats; a sequence of 36 or more triplets results in the production of a protein that has different characteristics called mutated huntingtin protein (mHtt, mutant Htt) and which will result in Huntington's disease [4], as it can be seen in figure 2.1.

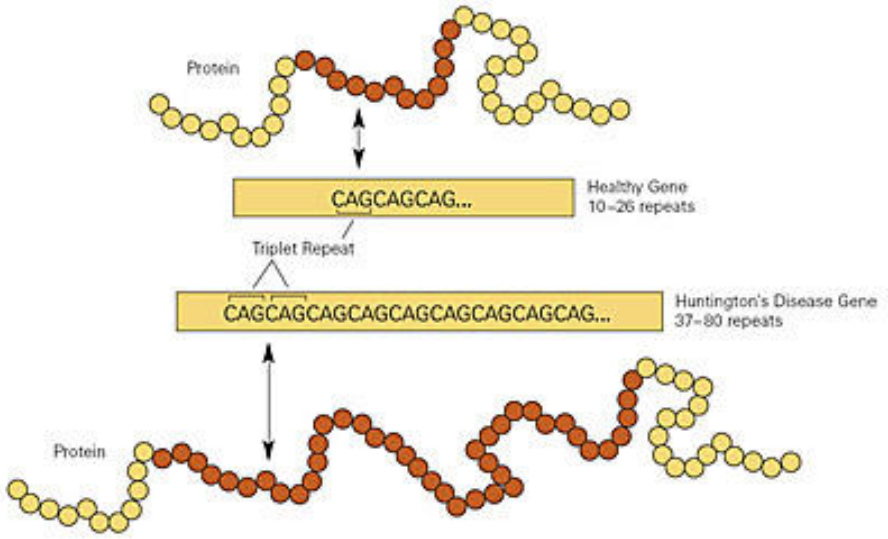

Figure 2.1: Two sequencies of CAG: the top one of a healthy person; the one below of a person with Huntington's disease.
Credit: National Institute of General Medical Sciences, National Institutes of Health

The Huntington's disease mutation is genetically dominant with near-complete penetrance: the mutation of one of a person's HTT genes causes the disease. One of the symptoms of the altered form mHtt is the death of some types of neurons in the brain and since the presence of these neurons is not uniformly distributed, different regions of the brain have a different involvement in this degeneration. Based on the number of CAG triplets in excess, the incidence of the disease is more or less accentuated. A number of repetitions ranging from 36 to 39 leads to a disease in the form of reduced penetrance, with a much later onset of age and with a slower progression. In a number of repetitions exceeding this threshold the disease has complete penetrance and can appear even at a young age, thus being defined as juvenile Huntington's disease. This accounts for approximately 7% of the conditions [5].
The behaviour of this mutated protein is not fully understood, but as

mentioned above it is evident that it is harmful to some types of cells, particularly those of the brain. The striatum is affected most early in symptoms, but as the disease progresses, other areas of the brain are also affected extensively. The disease brings with it a series of really serious complications for the sick subject, most of which due to the deterioration of muscle coordination and to a lesser extent, due to the behavioural changes induced by the progressive degeneration of cognitive faculties.
The greatest risk is of developing pneumonia (figure 2.2), which causes the death of half of those with Huntington's disease. Pulmonary compensation problems, the risk of inhaling food and drink and the increased likelihood of contracting pneumonia are the effects of the degenerative deterioration in the ability to synchronize movements. The second risk factor effect is the onset of heart disease, responsible for nearly a quarter of the deaths of people with the disease. Suicide is the third leading cause of death, with 7.3% of Huntington's disease sufferers taking their own life, while at least 27% attempt to do so. It has not yet been possible to understand whether the desire to commit suicide is due to psychiatric symptoms or the patient's willingness to avoid the later stages of the disease. Other causes of death from complications, albeit to a lesser extent, are related to suffocation, fall injuries and malnutrition [4].

2.1.3 Clinical Tests and Disease Course

The Unified Huntington's Disease Rating Scale (UHDRS)[6] is the most widely used clinical method for recording Huntington's disease and its progression. The UHDRS is the evaluation system to quantify the state of the disease and identify the stage of the sick subject. This method is divided into four sub-categories in order of relevance for the ability to identify the symptoms of the disease. The sections are: motor, cognitive, behavioural, functional. The final score is calculated by adding the various results obtained in the various sub-categories.
As mentioned, the motor symptoms are the most explanatory as they are the most robust and coherent ones and the quantification of these symptoms is indicated with a value, called Total Score System (TMS), obtained from the sum of 31 elements [7]. These elements are distributed among oculomotor functioning (6 elements), chorea (7 elements), dystonia (5 elements), bradykinesia (11 elements) and rigidity (2 elements) and each is rated on a 5-point scale ranging from 0 (severe impairment) to 4 (normal).
The second part of the motor assessment subsection consists of the Diagnostic Confidence Level (DCL), which is a single item with an ordinal rating scale of 5 categories. The examiner must choose a value based on how confident he is that the motor disturbance calculated by the TMS is

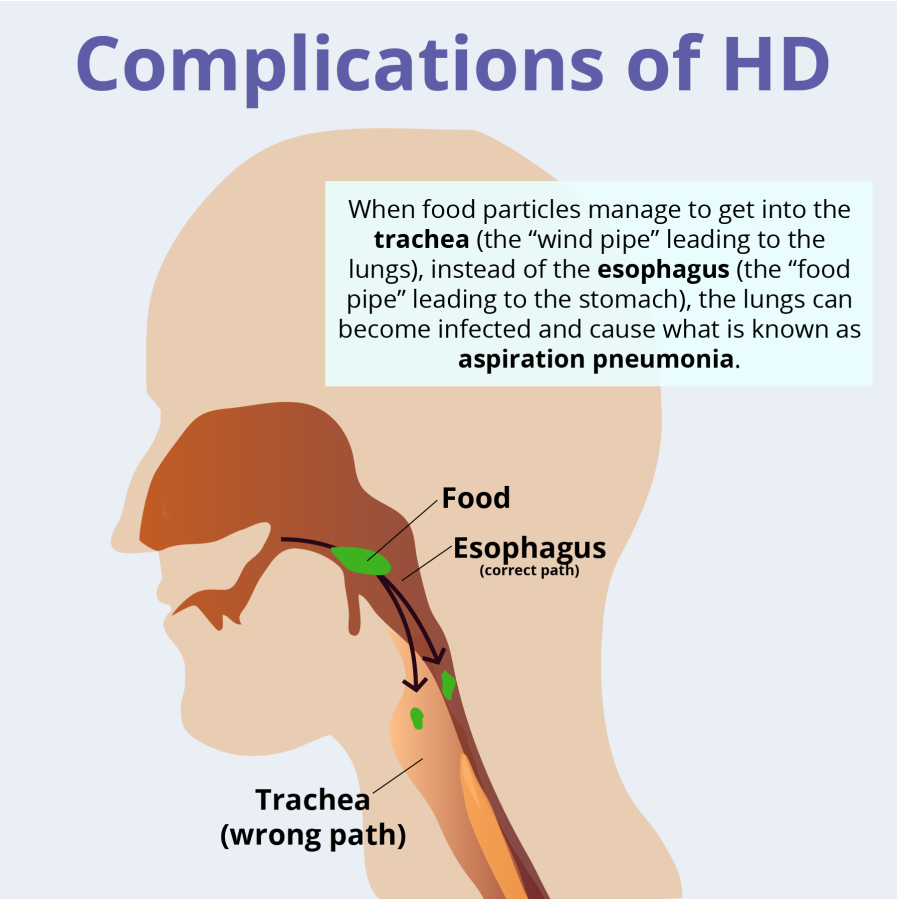

Figure 2.2: Pneumonia causes the death of half of those with Huntington's disease. Credit: Hopes Huntington's outreach project for education, at Stanford

due to Huntington's disease. Value 0 indicates that the patient is healthy and has no symptoms of the disease, value 1 indicates that the motor abnormalities are non-specific (<50% confidence), value 2 indicates that the abnormalities may be evidence of Huntington's disease (50% - 89% confidence), a value of 3 indicates that the motor abnormalities are likely signs of Huntington's disease (90% - 98% confidence interval) and a value of 4 indicates that the motor abnormalities are unambiguous signs of Huntington (>98% confidence)(see table 2.1).
Based on the results obtained from the UHDRS test, it is possible to divide the subjects examined into two main groups: premanifest and manifest. In the first group there are those presymptomatic subjects in which it is not yet possible to determine the onset of Huntington's disease while in the second group the subjects in which the symptoms of the disease are manifest and are classified into 5 stages based on the score obtained from TMS as indicated in table 2.2.

DLC	Description of syntoms
0	Normal
1	Motor abnormalities are non-specific
2	Abnormalities may be evidence of Huntington's disease
3	Motor abnormalities are likely signs of Huntington's disease
4	Motor abnormalities are unambiguous signs of Huntington

Table 2.1: DLC score

TFC	Years since onset	Stage
11 - 13	0 - 8	I
7 - 10	3 - 13	II
3 - 6	5 - 16	III
1 - 2	9 - 21	IV
0	11 - 26	V

Table 2.2: TFC relation with onset and division in stages

2.1.4 Atrophy and Thickness Reduction

As previously mentioned, one of the symptoms of Huntington's disease is the death of some neurons in the brain and the consequent atrophy of the brain organ. By cerebral atrophy we mean the reduction of the brain tissue, resulting from the necrosis and shrinking of the cells that make up the aforementioned tissue. Brain atrophy involves a loss of the functions performed by the brain. The extent of this loss depends on the extent of the brain areas affected by the processes of cellular necrosis and shrinkage. Through the analysis of magnetic resonances (MRI) it is possible to analyze the volumes and thicknesses of the brain structures through a longitudinal study (compare the measurements made on the same patient for a given period of time) and transversal (compare the measurements made by different patients). What emerges from these studies is that the rate of volume thinning is heterogeneous,

i.e. that the rate of atrophy is different in the different brain regions also as regards the time point in which degeneration begins [8].
Although heterogeneous, several studies have found that the state of atrophy, due to Huntington's disease, occurs mainly in the sub-cortical regions, where the most affected areas are the striatum and white matter [9].
These studies have also highlighted the close correlation between the striatal volume on the one hand and the age of onset and locomotor dysfunction on the other; the same is also true for white matter. Another cross-sectional study highlights that even in prodromal subjects (subjects presenting a non-specific clinical manifestation that appears anticipating the clinical picture typical of a given disease) it is possible to perceive differences between healthy and sick and that the loss of volume is mainly caused from thinning (figure 2.3).

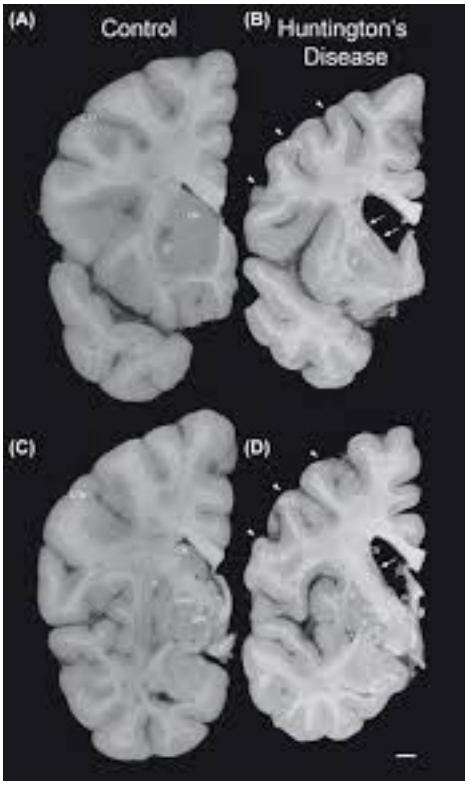

Figure 2.3: (A): right hemisphere of a healthy patient. (B): right hemisphere of a sick patient. (C): left hemisphere of a heathy patient. (D): left hemisphere of a sick patient. Credit: image taken from [10]

2.2 Magnetic resonance imaging

Magnetic resonance imaging (MRI) is an image generation technique used mainly in the medical field for diagnostic purposes, based on the physical principle of nuclear magnetic resonance. This imaging technique allows discrimination between different tissues on the basis of their biochemical composition, thus differentiating from other acquisition methods that do not allow such a distinction. MRI exploits the presence of hydrogen protons in the water contained in the body's tissues. A machine produces magnetic fields and radio frequency (RF) pulses that strike these hydrogen protons thus producing a signal that is returned to the machine and processed to obtain a high resolution image of the body tissue being analyzed. The result is images of the body sections on three different planes (axial, coronal, sagittal). Each voxel (3D pixel) of the image corresponds to a small area within this section. Based on the quantity and properties of the water present in an area, an intensity value will be stored inside the voxel which will uniquely identify that area, thus making it possible to distinguish different tissues from each other. Moreover, diseases, by affecting these tissues, modify the characteristics of the water very often, thus making it possible to distinguish a healthy tissue from a diseased one. The MRI can also be set, by adjusting some parameters, to obtain images with a different contrast to highlight the areas of analysis and different characteristics of these areas [11].

2.2.1 Structure and Operation

A commercial scanner for medical use is mainly made up of 4 elements that are used to create static and variable magnetic fields in time and space. Such elements are the main magnet, the radio frequency coils, the gradient coils and various auxiliary coils as it can be seen in figure 2.4. The main magnet, as the name implies, is the most fundamental component of the scanner and its purpose is to generate a constant magnetic field in space and time. The most important specification of a magnetic resonance imaging magnet is the strength of the field produced. Magnetic fields of greater intensity increase the resolution of the obtainable images and also decrease the time required for a scan. The radiofrequency coils, on the other hand, are necessary to create the rotating magnetic field at the Larmor frequency. The gradient coils are a fundamental part for a scanner as they have the function of generating magnetic fields that vary in space depending on how the current passing through them is modulated. Their primary characteristic is to obtain magnetic fields that vary linearly along one direction of the Cartesian axis and that are uniform in the other two. Around the main magnet there are also other coils in addition to the gradient coils, which have

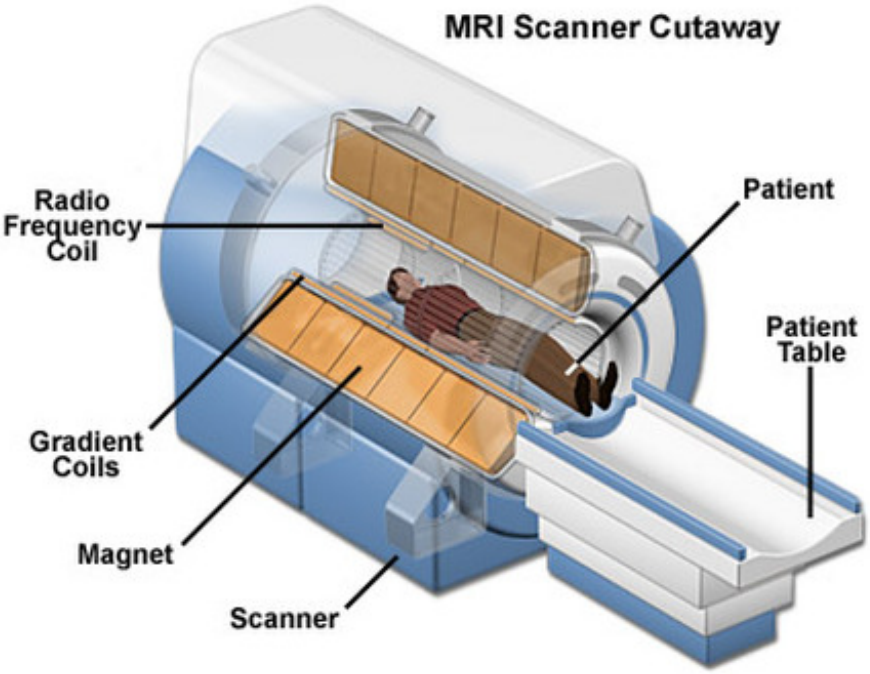

Figure 2.4: MRI machines.
Credit: MagLab

the function of improving the characteristics of the system itself.

2.2.2 Physics in Detail

The first step in creating an MRI image is to create a magnetic field, B_0, in such a way that the protons of the patient's body water respond to the magnetic field at the frequency f_0 and a part of these protons respond by creating a net magnetization, M, parallel to B_0.
This magnetization is initially uninteresting, as no apparent change is detectable. By rotating the net magnetization out of the equilibrium direction, a changing magnetic field will be generated which will induce a measurable signal usable for imaging. This is possible by applying a variable magnetic field B_1 in the plane perpendicular to the direction of B_0. When exposed to this new magnetic field, the vector M will begin to precess on it at the frequency $f_1 = (\gamma/2\pi)B_0$. But as soon as M is misaligned with B_0, (M) starts to precess around B_0 as well, at the resonant frequency f_0 with a corkscrew-like motion (figure 2.5); this implies rotation on both B_0 and B_1.
By applying a radio frequency (RF) pulse of the RF pulse it is possible to generate this magnetic field B_1. If two coils of wire (usually the same coils that are used to apply the RF pulse) are adjacent to the body,

they experience varying magnetic flux due to the rotating magnetization vector M. This varying magnetic flux will cause a current to flow in the wire.
When M is parallel to B_0, no current is induced in the receiver coils, as there is no change in the magnetic flux across the coil area. It is only when M is rotated in the transverse plane (xy) perpendicular to the static magnetic field that a signal can be generated due to the change in magnetic flux.

After explaining the way in which the signal is produced and the way

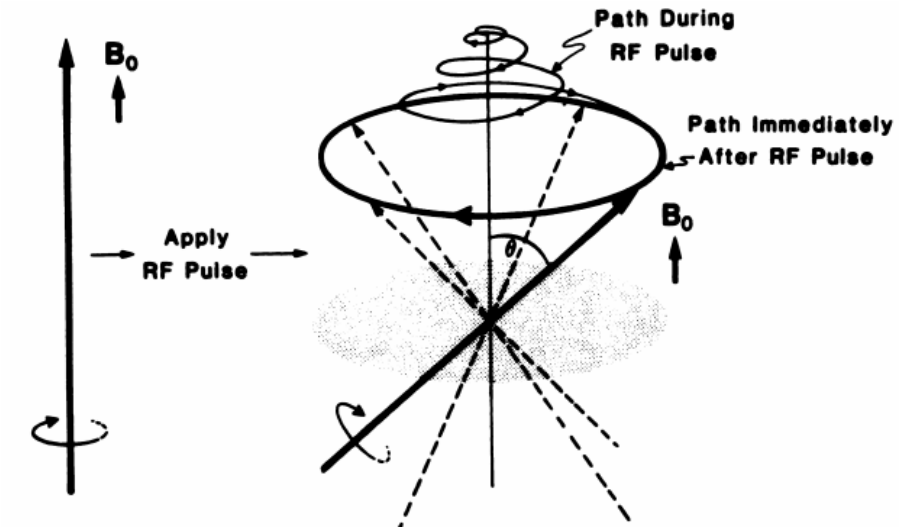

Figure 2.5: A short burst of B_1 in an RF pulse is capable of notating M out of the equilibrium direction by tracing out a spiral on the surface of a sphere with the tip of the M vector. Following the RF pulse the net magnetization vector will precess around the B_0 direction at the resonant frequency. Image taken from [12]

in which this signal affects the protons of the body's water, we will now analyze how the localization of the signal produced by the protons occurs and how this signal is captured in the voxel of the body final image. Thanks to a gradient-pulse sequence, a particular sequence of RF pulses and gradient magnetic fields it is possible to perform this localization of the signal.
First you need to select a slice and this is possible thanks to the use of the so-called slice selector gradient or G_{ss} . We know that the frequency of protons depends on their position with respect to the direction of B_0 and therefore with G_{ss}, which is added to B_0, we are able to modify the precession frequency of the protons in a predictable way. Thanks to the RF pulses produced by the MR machine within a specific frequency band length, it is possible to select only the slice we are interested in.
Three sets of gradient coils are used to be able to obtain the desired

orientation in space based on the tissue of the body we are analyzing. G_{ss} is nothing more than the combination of the magnetic fields produced by these gradient coils. The RF pulses and the slice selector gradient G_{ss} are closely related: in fact the RF bandwidth is directly proportional to the thickness of the slice, while the intensity of the gradient is inversely proportional to it. We can therefore obtain more or less thin slices in two ways, either by increasing the strength of the gradient G_{ss} or by reducing the bandwidth of the RF pulse.
After figuring out how to locate a slice, the next step is to locate every single point within the slice. This is possible by encoding each single signal into spatial frequencies and subsequently remapping these frequencies in the two-dimensional spatial domain through the 2D inverse Fourier transform.
The spatial frequency domain is called $k - space$ where k indicates the number of dimensions of the space. In our case, since we are working on a slice in two dimensions, k will be equal to two and since we are in the presence of a discrete domain it is possible to imagine this $2 - space$ as a matrix within which each cell is identified through two spatials frequencies, one for each direction in the slice (figure 2.6).
Two gradients are used to encode the signal: a phase encoding gradient

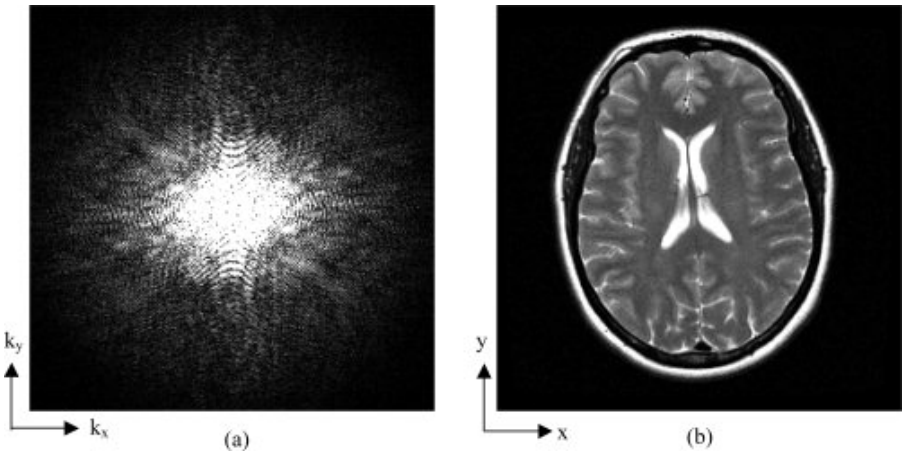

Figure 2.6: On the left (a) the representation of an MRI image in the $k - space$, on the right (b) a MRI image representing a slice.
Credit: image taken from [13]

(G_{pe}), applied after slice selection, and a frequency encoding gradient (G_{fe}), applied continuously during signal acquisition. The two gradients are not used at the same time but first the selection of the row/column takes place based on the direction in the slice where G_{pe} is applied, thanks to the activation of G_{pe}.
In fact, after the RF pulse is activated all the protons are in phase and therefore all the protons of the selected slice produce a signal. Thanks to

the activation of the G_{pe} gradient it is possible to modify the precession frequency of the protons according to their position.
After deactivating G_{pe}, only a small part of the protons will correspond to a certain spatial frequency and therefore only these will contribute to the measured signal. In this way we were able to select a row/column. G_{fe} is then activated and will remain on for the duration of the signal acquisition. As for all the other gradient fields, G_{fe} has the function of modifying the precession frequency of the protons according to their position and therefore to interrogate more spatial frequencies and to obtain an image with more resolution in the G_{fe} direction it is necessary to increase the frequency of sampling. In this way we were able to identify each point of a specific row/column; to be able to map all the rows/columns you have to repeat the procedure applying a different G_{pe} each time.
To clarify the procedure, let's take the example of being in a $k-space$ of 512×1024, where G_{pe} is applied in the horizontal direction, identifying the columns, while G_{fe} is applied in the vertical direction, locating the rows. It therefore becomes necessary to use 1024 different G_{pe}: each gradient applied corresponds to a specific column of the $k-space$. The signal is sampled 512 times while G_{fe} remains active: each sample corresponds to a specific line of the $k-space$. For further information see [12, 11].

2.2.3 MRI Limitations

After scanning through an MR machine we are able to obtain high resolution images of slices of the tissue/organ we are analysing. These images, although very precise, are certainly not without errors; it is possible to find different types of errors such as misalignment, out-of-scale values or unwanted data (for example fabrics that do not interest us for analysis). These errors are easily localized by the eye of an expert but if we want to use these data to process them in a calculator, a data "cleaning" step is necessary so that the analyses are not affected by the errors mentioned above.
Another intrinsic problem to MRI is the fact that it can only return two-dimensional (2D) images, instead for our analysis it is necessary to have three-dimensional (3D) images in order to apply the functional maps algorithm to our case of analysis.

2.2.4 Freesurfer

FreeSurfer is free software, developed by Harvard University, specifically for the study of the brain and its cortical and subcortical anatomy. Much of FreeSurfer's pipeline is automated to greatly simplify analysis on a large amount of data.

The software is able to reprocess the images obtained through MRI and to build models of the white matter, the cortical gray matter and the pial surface. After the construction of these three-dimensional models it is possible to carry out different anatomical measurements such as: cortical thickness, surface area, curvature, the normal to the surface at each point of the cortex, etc.
In addition to being able to perform these operations, the software is able to deform these surfaces to have a better view of the affected areas. It is possible to divide the steps performed by FreeSurfer into two main phases, the first deals mainly with the original MRI volumes, while the second works with the surfaces obtained in the first step. The first step is designed to reprocess the MRI volumes is to identify and label the subcortical tissue classes. This procedure is divided into 5 basic steps [14]. Summarizing the various steps, the MRI volumes are recorded via an affine transformation designed to be insensitive to disease and to maximize the accuracy of the final segmentation and is subsequently labeled. These steps are solely dependent on skull stripping [15] to create a brain mask in which labeling is performed (figure 2.7). In the

Figure 2.7: An example of MRI labelled volume after the first step

second phase instead, FreeSurfer uses the models created previously to extract the cortical and subcortical surfaces and all the information related to them [16, 17]. Voxels are first classified as white matter or as

something that is not white matter based on the intensity of the voxels. We then proceed by separating the two hemispheres of the brain based on the symmetry of the white matter and on algorithms that encode the expected shape of these structures and by removing the cerebellum and the brain stem.
An initial surface is then generated for each hemisphere by tiling the outside of the white matter mass for that hemisphere. This initial surface is then smoothed following the intensity gradients between the white matter and the gray matter, obtaining the definitive white surface (figure 2.8), which is moved to be able to identify the pial surface (figure 2.9.
It was done in the same way as before but refining the surface by suiting the intensity gradients between the gray matter and the cerebrospinal fluid. The distance between the white and the flat surface gives us the resulting thickness [18]. We can also calculate the local curvature, the surface area and the surface normal.

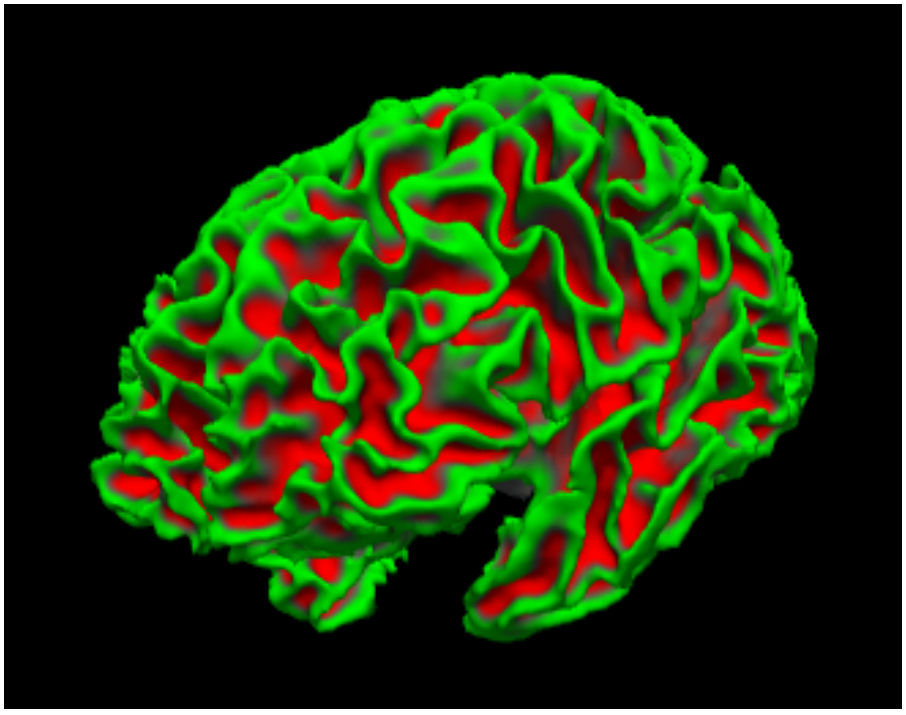

Figure 2.8: An example of white surface after the second step

2.3 Functional Maps

The main goal of shape matching is to find a point-to-point correspondence between two shapes which are usually represented as point clouds

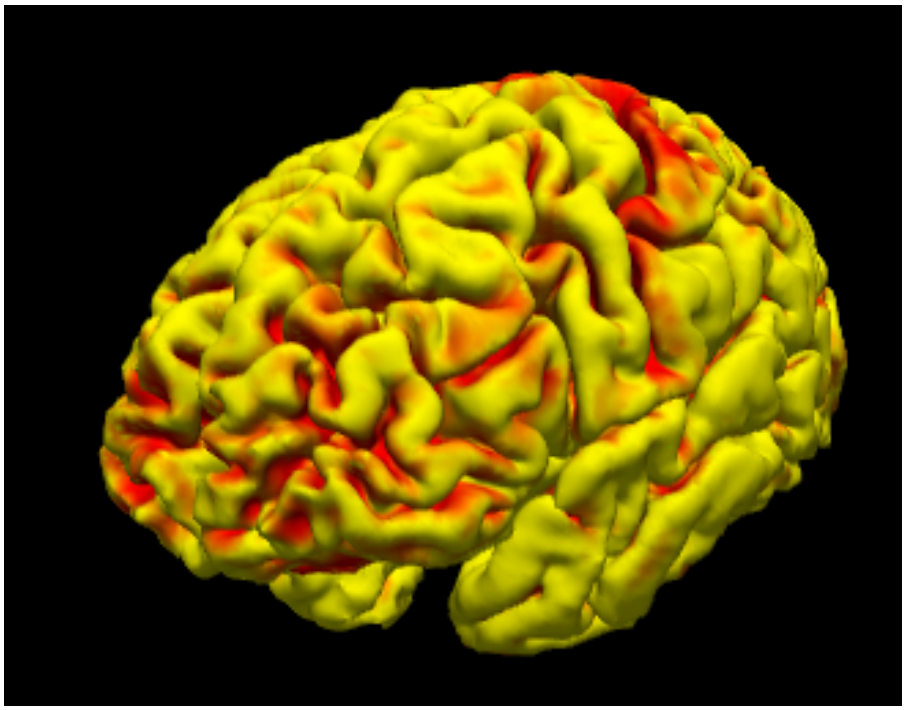

Figure 2.9: An example of pial surface after the second step

or polygon meshes. A classic approach is to find a correspondence map that connects the sets of points that make up the two shapes.
The approach used within the thesis aims to consider the mappings between functions defined on the shapes, rather than inserting points of correspondence on the shapes [19, 20]. This approach can be considered as a generalization of the classical point-to-point map since at each point-to-point correspondence it induces a mapping between function spaces. However, this generalized representation is both suitable for shape matching as many natural constraints on the map become linear constraints on the functional map, and flexible in choosing the basis for the function space on each shape.
The choice of the eigenfunctions of the Laplace-Beltrami operator allows to benefit from their multi-scale, "geometry aware" nature. Basically, the possibility of using a small number of Laplace-Beltrami bases for the spaces of the functions of the two forms, allows to create a map (figure 2.10(a)) that can be approximated to a relatively small matrix with respect to the total number of points constituting the forms, which is identified as C (figure 2.10(b)).

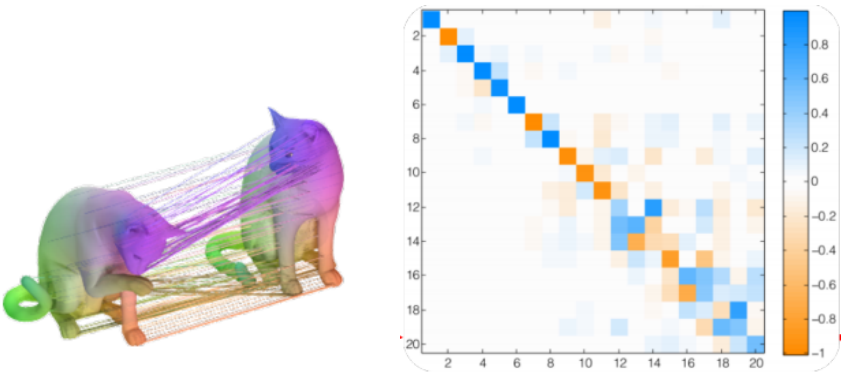

(a) Point-to-point correspondences obtained by Functional Maps algorithm

(b) Matrix C encoding the map

Figure 2.10: Results with Functional Maps using Tosca dataset (a) with the relative matrix C (b).
Credit: image taken from [19]

2.3.1 Laplace-Beltrami Operator

To be able to create a finite matrix C of relatively small dimensions that represents a transformation T_F in a compact way, I need to use a relatively small subset of basic functions. The starting choice is to use basic functions ϕ_i^M on the form M and ϕ_j^N on the form N, but I need to satisfy two fundamental requirements: compactness and stability.
The first because the simplest elements of a form must be represented with the fewest possible basic functions and the second because the space of functions extended by the linear combination of the basic functions must be stable with reference to small deformations.
In differential geometry, the Laplace-Beltrami operator is a self-adjoint differential operator that generalizes the Laplace operator to functions defined on Riemannian manifolds. A Riemannian manifold is a differentiable manifold (curve or surface) on which the notions of distance, length, geodesics, area (or volume) and curvature are defined.
The manifold is a topological space locally similar to a well known topological space such as the Euclidean one but which globally can have different geometric properties such as being curved. The Laplace-Beltrami operator is therefore the extension to non-Euclidean cases of the standard Laplacian and can be discretized. The most interesting feature of the eigenfunctions of this operator is that its eigenfunctions are parallel to the Fourier bases and how the latter are ordered according to their absolute value; this makes these eigenfunctions suitable for the T_F transformation since, being ordered from the lowest to the highest frequency, they provide an innate multiscale way to approximate functions. The transformation matrix of the Fourier coefficients, compact

and optimizable, therefore represents the functional map.
This optimization is based on the alignment of a set of functions which can be calculated on both forms and which are known to correspond to each other. So the first thing needed to exploit this method is to compute a set of descriptors for each point on both forms, M and N, and then create some function conservation constraints from them. On the basis of the forms between which we have to make shape matching, it is possible to use different types of descriptors that can be better adapted to the specific case.
In a general case it is possible to use two descriptors that fit more or less well to any shape: the Wake Kernel Signature (WKS) [21] and the Heat Kernel Signature (HKS) [22]. WKS exploits the Schrodinger wave equation to characterize a point $x \in X$ from the mean probabilities of quantum particles of different energy levels to be measured in x. Since the energies of the particles correspond to the frequencies, in this approach information from all frequencies is captured while at the same time the influences from the different frequencies are clearly separated. The Wave Kernel Signature (WKS) can be defined as

$$w(E, x) = \sum_{i=0}^{n} \phi_i(x)^2 f_E(\lambda_i)^2 \tag{2.1}$$

where E is an approximation of the energy expected value, and $f_E(\lambda_i)^2$ is an energy probability distribution. Similarly, Heat Kernel Signature instead uses the heat diffusion equation to characterize a point $x \in X$ for the amount of heat measured in x at certain times $t > 0$. The Heat Kernel Signature (HKS) can be computed as

$$h(x, t) = \sum_{i=0}^{n} e^{-\lambda_i t} \phi_i^2(x) \tag{2.2}$$

where λ_i, ϕ_i are eigenvalues and eigenfunctions of the Laplace Beltrami operator eigendecomposition and n is the number of selected eigenfunctions.
To set the stage for functional mappings as a generalization of classical point-to-point mappings, let $T : M \to N$ be a bijective mapping between manifolds M and N.
If we are given a scalar function $f : M \to \mathbb{R}$ then we obtain a corresponding function $g : N \to \mathbb{R}$ by composition, as in $g = f \circ T^{-1}$.
We use $\mathcal{F}(\cdot, \mathbb{R})$, a generic space of real-valued functions, to denote this trasformation $T_F : \mathcal{F}(M, \mathbb{R}) \to \mathcal{F}(N, \mathbb{R})$. We call T_F the functional representation of the mapping T. We know that the original mapping T can be recovered from T_F and that for any fixed bijective map $T : M \to N$, T_F is a linear map between function spaces.

We may paraphrase these remarks to say that knowledge of T_F is equivalent to knowledge of T. And while T may be a complicated mapping between surfaces, T_F acts linearly between function spaces.
Every function $f : M \to \mathbb{R}$ can be represented as a linear combination of basis functions ϕ_i^M as $f = \sum_i a_i \phi_i^M$.
In the same way I can also apply to N a set of basis functions ϕ_j^N, doing so I can consider $T_F(\phi_i^M) = \sum_j c_{ij} \phi_j^N$ for some c_{ij} and

$$T_F(f) = \sum_i a_i \sum_j cij\phi_j^N = \sum_i \sum_j a_i c_{ij} \phi_j^N \tag{2.3}$$

as can be seen in Figure 2.11.

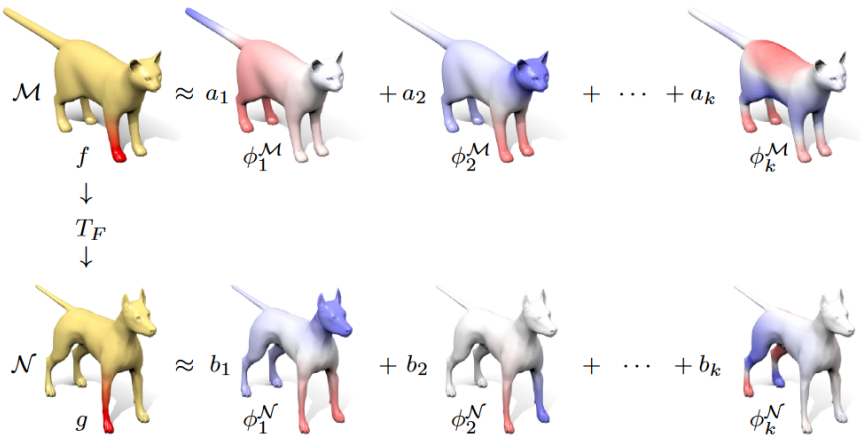

Figure 2.11: Basis functions applied to source shape M and target shape N. Credit: image taken from [19]

2.3.2 Functional Matrix C

Let ϕ_i^M and ϕ_j^N be bases for $\mathcal{F}(M, \mathbb{R})$ and $\mathcal{F}(N, \mathbb{R})$, respectively. A generalized linear functional mapping $T_F : \mathcal{F}(M, \mathbb{R}) \to \mathcal{F}(N, \mathbb{R})$ with respect to these bases is the operator defined by (2.3) where $c_i j$ is a possibly infinite matrix of real coefficients (subject to conditions that guarantee convergence of the sums above).
If now we consider f as a vector of coefficients $\mathbf{a} = (a_1, a_2, \dots, a_i, \dots)$ and $g = T_F(f)$ as another vector of coefficients $\mathbf{b} = (b_1, b_2, \dots, b_i, \dots)$ then, we can rewrite the equation mentioned above in (2.3) as

$$b_j = \sum_i a_i c_{ij} \tag{2.4}$$

where c_{ij} is completely independent from the chosen function and is

determined only by the bases and the map T.
The map T_F can be represented as a (possibly infinite) matrix C s.t. for any function f represented as a vector of coefficients $\mathbf{a}$ then $T_F(\mathbf{a}) = C\mathbf{a}$.
This remark in combination with the previous two remarks shows that the matrix C fully encodes the original map T.
In addition to this, if the shapes M and N are isometric and T is an isometry, matrix C_{ij} can be non-zero only if ϕ_i^M and ϕ_j^N correspond to the same eigenvalue. In particular, if all eigenvalues are non-repeating, matrix C will be diagonal.
If the trasformation T is not an isometry, so the shapes M and N are non-rigidly deformed, the matrix C is not yet diagonal but it still close to it with a funnel shape that stays along the diagonal. It is necessary underline that the matrix C stops to be diagonal or close to diagonal when the non-isometric deformations are not so small and it is mostly visible at high frequencies eigenfunctions (at the bottom-right corner of the matric C).

2.3.3 Functional Maps Inference

Functional shape maps are well-suited for inference because of their continuous nature and because a large number of constraints become linear in this representation. Suppose we are given a pair of discrete shapes represented as meshes, with the corresponding Laplace-Beltrami eigenfunctions. As we have seen, the goal of this method is to find the underlying functional map represented as a matrix C that matches the trasformation T from the shape M and the shape N. The simplest way to do so is to construct a large system of linear equations, where each equation corresponds to one of the constraints. These constraints can be either a functional constraint or the operator commutativity constraint.Then, it is possible to find the best functional map by finding the matrix C that best satisfies the constraints in the least squares sense. A list of the steps necessary to do this is presented at algorithm 1.

Algorithm 1 Functional Maps Inference for Matching

Compute a set of descriptors for each point on M and N, and create function preservation constraints.
If landmark correspondences or part decomposition constraints are known, compute the function preservation constraints using those.
Include operator commutativity constraints for relevant linear operators on M and N (e.g. Laplace-Beltrami or symmetry).
Incorporate the constraints into a linear system and solve it in the least squares sense to compute the optimal C.
Refine the initial solution C using one of the iterative methods proposed below.

Figure 2.12: Some other results obtained by Functional Maps

2.3.4 Post-Processing Iterative Refinement

One of the method used to improve and refine the algorithm presented and the method used for the thesis is the standard Iterative Closest Point (ICP) algorithm of Besl and Mckay [23] with the only difference that in this case it is applied in the spectral embedding rather than on the simple Euclidean space.
We have the two matrices of the Laplace-Beltrami eigenfunctions Φ^M and Φ^N that refers to M and N. Every colums of these matrices corresponds to a point and every row corresponds to an eigenfunction; so it is possible to obtain the image of the function centered in each point of M simply as $C\Phi^M$.
Given an initial estimate matric C_0 that represents a point-to-poiny map T. We have understood that each colums of the matrix obtained by $C_0\Phi^M$ coincides theoretically with same colums of Φ^N. C_0 must align Φ^M and Φ^N since we consider these as two point clouds with dimensionality equal to the number of eigenvalues used in the functional representation C_0.
Thus an iterative refinement of C0 can be obtained via simple iterative cycle of steps:

1. For each column x of $C_0\Phi^M$ find the closest $\bar{x}$ in Φ^N.
2. Find the optimal orthonormal C minimazing $\sum ||Cx - \bar{x}||$.
3. Set $C_0 = C$ and iterate until convergence..

To obtain a good refinement of the initial matrix C_0, it is essential to have a good initial estimate C_0.
Finally, note that the output of this procedure is not only a functional matrix C but also a point-to-point correspondence given by nearest neighbor assignment between points on M and N.

Chapter 3

Thickness Analysis

In this chapter I intend to explain in detail how I set up the core of the thesis, trying to be as exhaustive and complete as possible.
The goal of my research is to compare, thanks to the analysis of the available data, the thickness of the brains taken in the study and to classify, through the use of automated algorithms, healthy patients from patients in which Huntington's disease is in an embryonic state.
My thesis compares two methods to achieve this and highlights what they consist of and what differentiates them from each other showing the usefulness and effectiveness of one over the other or vice versa.
The two methods will presented separately one after the other.

3.1 Problem Formulation

Thanks to the use of the Freesurfer software, it was possible to obtain from the MRI images of the patients, a high-resolution volumetric reconstruction of the hemispheres of the patients' brains. After the construction of these three-dimensional models it was possible to carry out various anatomical measurements such as: cortical thickness, surface, curvature, normal to the surface in each point of the cortex. One of the main symptoms of Huntington's disease, as mentioned in chapter 2, is the reduction of brain tissue, resulting from the necrosis and shrinkage of the cells that make up the aforementioned tissue. It therefore becomes possible to perceive differences between a healthy patient and a sick patient from the loss of volume caused mainly by thinning. Consequently, the most interesting anatomical measurement to be analyzed was cortical thickness.
A cross-sectional study (visits of different patients) and a longitudinal study (visits of the same patient after about one year) are available. In this way it was possible to extract the values of the cortical thickness both for different patients and for the same patient for years later. From

the analysis of these data, the goal is to classify healthy patients from those affected by the first symptoms of Huntington's disease thanks to a study on the patients' cortical thickness. Thickness can be seen as a function f_i^u such that:

$$f_i^u : S_i^u \longmapsto \mathbb{R} \tag{3.1}$$

where f_i^u stands for the values of the thickness for the patient u at the visit i and S_i^u stands for the white surface of the brain of patient u at the visit i.
The goal is to classify, through the thickness function, healthy patients (*control*) from those affected by the first symptoms of Huntington's disease (*earlyHD*):

$$C : \{f_1^u, ..., f_n^u\} \longmapsto \{earlyHD, control\} \tag{3.2}$$

My thesis aims to analyze and compare two methods that both use the thickness function but implementing a different brain registration. The first method, through the use of Freesurfer, allows to carry out a global registration, patient indipendent, of all the brains:

$$R_i^u : S_i^u \longmapsto R \tag{3.3}$$

where R stands for the global registration indipendent from the patients. The second method, through the use of Functional Maps algorithmn, allows, instead, to carry out a user-specific registration, based on patients brain:

$$F_i^u : S_i^u \longmapsto S_0^u \tag{3.4}$$

where F_i^u stands for the user-speficic patient registration.

3.2 Freesurfer Data Analysis

In this section I will present the first method that I used to compute Freesurfer data on brain. I will present it in such a way that all the are clear and exhaustive. The results obtained by this method will then be presented in chapter (5) and compared with those obtained by the other.

3.2.1 Evaluation of Thickness

The first step to be performed is to extract the cortical thickness values from the three-dimensional models created thanks to the use of Freesurfer. The result of this operation is the acquisition of a vector containing a thickness value for each point of the three-dimensional model of the patient's white surface.
Having available a longitudinal study with a variable number of visits

from four for presymptomatic patients and seven for healthy patients, a vector is saved for each patient for each time instant. In this way I have a vector containing the thickness values (for each three-dimensional point) for each patient under analysis and for each time. Each time instant corresponds to a different visit made by the patient and can be indicated with V^t where $t = 1, 2, 3, 4, 5, 6, 7;$.
It will therefore be possible to analyze the difference in thickness between the various pairs (V^t, V^1) with $t = 1, 2, 3, 4, 5, 6, 7;$ and verify if the increase of this difference (due to a lower thickness in the visits after the first) is accentuated in the case of a patient in which the first symptoms of disease begin to appear compared to healthy patients. To show how much the thickness decreased between a V^t visit and the first visit V^1, I choose to sum the absolute value of each difference in thickness, calculated as

$$\Delta th = \sum_{n=1}^{n} |V_n^t - V_n^1| \tag{3.5}$$

where n is the number of points in the model shape.
I choose to use the absolute value as it is not possible for the white matter to increase with the progress of time and therefore with the aging of the patient. Furthermore, I decided to sum all the values because, as mentioned in chapter 2, practically all areas of the brain are affected by necrosis of the brain tissue.

3.3 Functional Maps on Cerebrums

In this section I will present the method that makes use of the Functional Maps algorithm, presented in chapter 2, and how it was adapted for my brain analysis. I will present all the passages clearly and exhaustively. The results obtained by this method will then be presented in chapter (5) and compared with those obtained by the other. Since I have both a

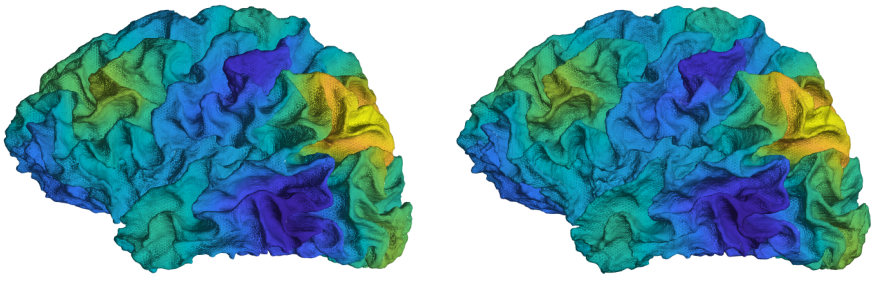

(a) Source shape M (b) Target shape N

Figure 3.1: Functional Maps on source shape (a) and target shape (b).

transversal study and a longitudinal study, I use the method of functional maps to find a map that represents the correspondences between real-valued functions on the hemispheres of the same patient but scanned in different time periods. From this map it is therefore possible to extract a point-to-point correspondence in a very simple way that allows to obtain a method of transferring the functions between the shapes, given by the point-to-point map. In this way it is possible to obtain a registration of the brains that is not global (as in Freesurfer) but specific for each patient which allows to transfer the thickness function from one shape to another.
In particular, a functional map will be found for each available time interval.
Assuming we have four visits, V_1, V_2, V_3, V_4, which represent the visits at time $t = 1, 2, 3, 4$; , we will look for the correspondences between the pairs (V_1, V_2), (V_1, V_3), (V_1, V_4). In this way the functional map will change according to the degeneration / non-degeneration of the patient's brain and consequently will transfer the thickness function more or less precisely.
It will then be possible to analyze the difference in thickness between the various (V_1, V_2), (V_1, V_3), (V_1, V_4) pairs and verify whether this reduction is accentuated in the case of a patient in which the first symptoms of disease begin to arise compared to healthy patients.

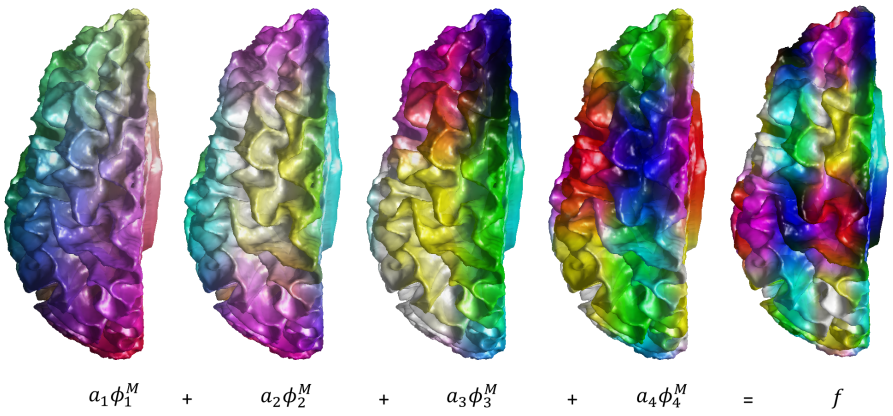

Figure 3.2: Basis functions ϕ_i^M applied on source shape M

3.3.1 Choice of Basis Functions

From now on, for each pair of visits (V_1,V_i), the source shape of V_1 will be indicated as M and the target shape of V_i as N. The first step, but of fundamental importance, to correctly apply the Functional Maps algorithm to shapes M and N, is the choice of the basis functions.

There are two properties, as mentioned in chapter 2, that must be respected: compactness and stability. By compactness we mean the ability to approximate the natural functions applied to the shape with a small number of basis functions; by stability we mean that the space of functions spanned by the linear combination of the basis functions must be robust to small deformations. The natural choice therefore was to use the eigenfunctions of the Laplace-Beltrami operator as basis functions because on the one hand, behaving like Fourier basis, they are ordered according to their frequency (from lower frequencies to higher frequencies) and therefore using only a limited set of the former it is possible to approximate well the starting functions, and on the other hand, being able to represent periodic functions as a linear combination of sinusoidal functions, they allow to obtain the desired stability.
In order to get a square matrix, I decided to use the same number of eigenfunctions on the shape M and on the shape N.
ϕ_i^M are the basis functions on shape M and ϕ_j^N are the basis functions on shape N, where $i = j$.
The basis function can represent every function $f : M \to \mathbb{R}$ as a linear combination as $f = \sum_i a_i \phi_i^M$ as it can be seen in figure 3.2.
Applying to N a set of basis functions ϕ_j^N, thus getting $T_F(\phi_i^M) = \sum_j cij\phi_j^N$, for some c_{ij} and I get:

$$T_F(f) = \sum_i a_i \sum_j c_{ij}\phi_j^N = \sum_i \sum_j a_i c_{ij}\phi_j^N \tag{3.6}$$

If now we consider f as a vector of coefficients $\mathbf{a} = (a_1, a_2, \dots, a_i, \dots)$ and $g = T_F(f)$ as another vector of coefficients $\mathbf{b} = (b_1, b_2, \dots, b_i, \dots)$ then, we can rewrite (3.6) as $b_j = \sum_i a_i c_{ij}$ where c_{ij} is completely independent from the chosen function and is determined only by the bases and the map T.
The map T_F can be represented as a matrix C s.t. for any function f represented as a vector of coefficients $\mathbf{a}$ then $T_F(\mathbf{a}) = C\mathbf{a}$.

3.3.2 Computing the Descriptors

My choice was to select a small number of landmarks (six to be precise) uniformly distributed on shapes M and N. These landmarks have been saved in two vectors l^M and l^N respectively for shape M and shape N. Given two associated sets of landmarks, I need to compute a set of descriptors for each point x in l_x^M and in l_x^N. I decided to use Wake Kernel Signature (WKS): the basic idea is to characterize each landmark x in l_x^M based on the average probabilities of quantum particles of different energy levels to be measured in x. Since the energies of the particles correspond to the frequencies, in this approach information

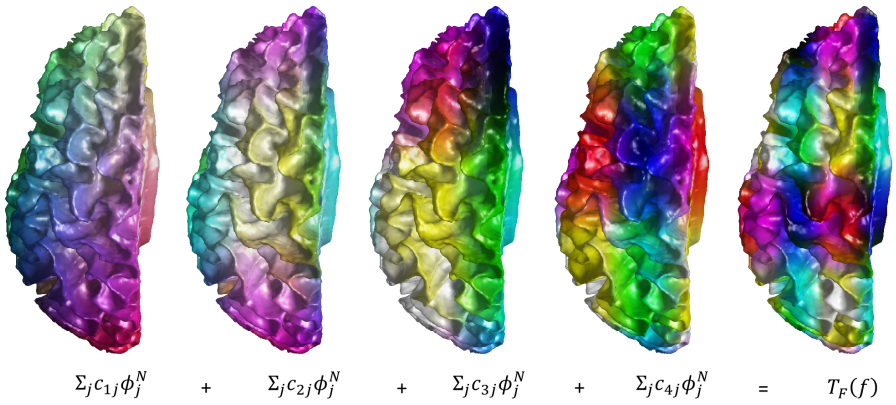

Figure 3.3: Basis functions ϕ_j^N applied on target shape N

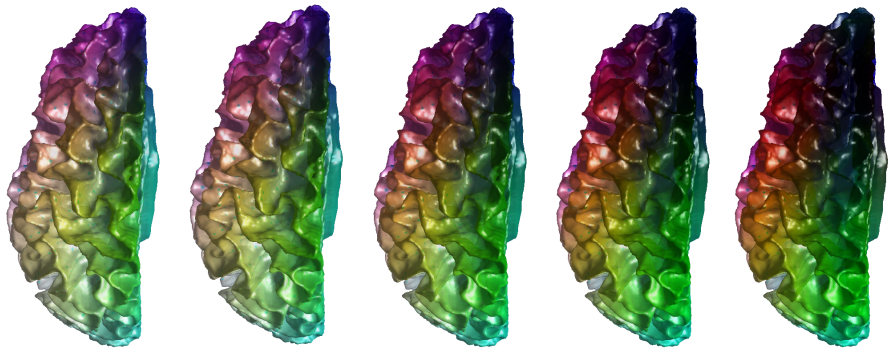

Figure 3.4: First 5 steps of temporal evolution of the wave equation on source shape M

from all frequencies is captured while at the same time the influences from the different frequencies are clearly separated.

First of all, I need to determine the probability of measuring a quantum particle of a certain energy distribution in a given location. The evolution of a quantum particle on the surface is governed by its wave function $\psi(l_x^M, t)$ which is a solution of the Schrodinger equation, a phisic fundamental equation that determines the temporal evolution of the state of a system:

$$\frac{\delta\psi}{\delta t}(l_x^M, t) = i\Delta\psi(l_x l^M, t) \tag{3.7}$$

For example, I take a quantum particle with unknown position is on the shape M. At time $t = 0$ I can make an approximate measurement of its

Algorithm 2 Wave Kernel Signature WKS

Input : $l_x^M, l_x^N, \phi_k^M, \phi_k^N$
Output : Fct_x^M, Fct_x^N

1 $\psi_E(l_x^M, t) = \sum_{k=0}^{\infty} e^{iE_k t}\phi_k(l_x^M) f_E(E_k)$ // The wave function of a quantum particle in the coordinates l_x^M in the shape M

2 $\psi_E(l_x^N, t) = \sum_{k=0}^{\infty} e^{iE_k t}\phi_k(l_x^N) f_E(E_k)$ // The wave function of a quantum particle in the coordinates l_x^N in the shape N

3 $WKS(E, l_x^M) = \lim_{T\to\infty} \frac{1}{T}\int_0^T |\psi_E(l_x^M, t)|^2$ // Define the WKS as the average probability of the energy to measure a particle in l_x^M

4 $WKS(E, l_x^N) = \lim_{T\to\infty} \frac{1}{T}\int_0^T |\psi_E(l_x^N, t)|^2$ // Define the WKS as the average probability of the energy to measure a particle in l_x^N

5 $Fct_x^M = WKS(E, l_x^M) = \sum_{k=0}^{\infty} \phi_k(l_x^M)^2 f_E^2(E_k)^2$ // $e^{-iE_k t}$ are orthogonal for the L^2 norm

6 $Fct_x^N = WKS(E, l_x^N) = \sum_{k=0}^{\infty} \phi_k(l_x^N)^2 f_E^2(E_k)^2$ // $e^{-iE_k t}$ are orthogonal for the L^2 norm

energy E.
I decided to do this choice because this allow me to cope with perturbations of eigenenergies under non-rigid deformation of the shape M. Doing this approximation we obtain a certain probability distribution f_E^2 with expectation value E.
In the case of the study the Laplace spectrum of the shape M has no repeated eigenvalues, then the wave function of the particle is given by

$$\psi_E(l_x^M, t) = \sum_{k=0}^{\infty} e^{iE_k t}\phi_k(l_x^M) f_E(E_k) \tag{3.8}$$

The probability of measuring the particle at point l_x^M is therefore $|\psi_E(l_x^M, t)|^2$.
I choose to not consider time because it has no straightforward interpretation in the geometrical characteristics of the shape. The eigenvalues of the Laplace-Beltrami operator is strictly related to energy and therefore to an intrinsic notion of scale in the shape M, so I decide to replace the time with the energy defining the WKS as the average probability (over time) to measure a particle in l_x^M:

$$WKS(E, l_x^M) = \lim_{T\to\infty} \frac{1}{T}\int_0^T |\psi_E(l_x^M, t)|^2 \tag{3.9}$$

Since the functions of $e^{-iE_k t}$ are orthogonal for the L^2 norm, simply substituting Equation (3.8) into Equation (3.9) I obtain for shape M

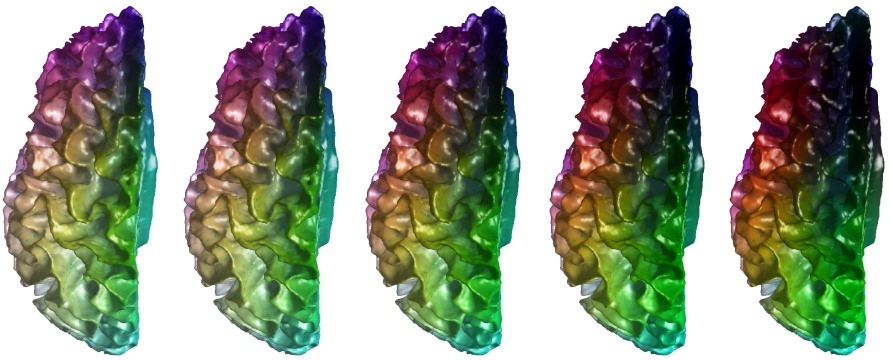

Figure 3.5: First 5 steps of temporal evolution of the wave equation on target shape N

and N respectively:

$$\begin{aligned} Fct_x^M &= WKS(E, l_x^M) = \sum_{k=0}^{\infty} \phi_k(l_x^M)^2 f_E^2(E_k)^2 \\ Fct_x^N &= WKS(E, l_x^N) = \sum_{k=0}^{\infty} \phi_k(l_x^N)^2 f_E^2(E_k)^2 \end{aligned} \tag{3.10}$$

The eigenvalues of the Laplace-Beltrami operator is strictly related to energy and therefore to an intrinsic notion of scale in the shape M. To derive a descriptor which characterizes the properties of the shape at different scales independently we merely need to choose the appropriate distributions f_E^2 in (3.10) , and to define an appropriate distance between wave kernels.

3.3.3 Matrix C

Finally, I have all the elements that I need to compute the functional matrix C, that represents the transformation T_F from the source shape M to the target shape N.
The simplest method for recovering an unknown functional map between M and N shapes is to solve the following optimization problem:

$$C = \min_P \sum_x \| PFct_x^N - Fct_x^M \|_F^2 + \alpha \sum_k \| \phi_k^M P - P\phi_k^N \|_F^2 \tag{3.11}$$

where Fct_x^N are the wake kernel descriptors computed with (3.10) of source shape M, Fct_x^M are the wake kernel descriptors computed with (3.10) of the target shape N, ϕ_k^M are the k selected Laplace-Beltrami eigenfunctions on the souce shape M, ϕ_k^N are the k selected Laplace-Beltrami eigenfunctions on the target shape N and α is a scalar weight

parameter. As the shapes are approximately isometric and the descriptors are well-preserved by the (unknown) map, then this procedure already gives a good approximation of the underlying map.
The second part of the optimization function is called *Operator Commutativity Constraint* and assert that, given functional operator, as Laplace-Beltrami eigenfunctions, on shapes M and N it may be natural to require that the functional map C commute with ϕ_k^M and ϕ_k^N respectively. After the optimization problem, I obtain a functional maps C of size $k \times k$ that encodes the transformation from the functional space of N to that of M as in equation (3.11). It is possible to see a graphical representation of matric C of size 60×60 in figure 3.6.

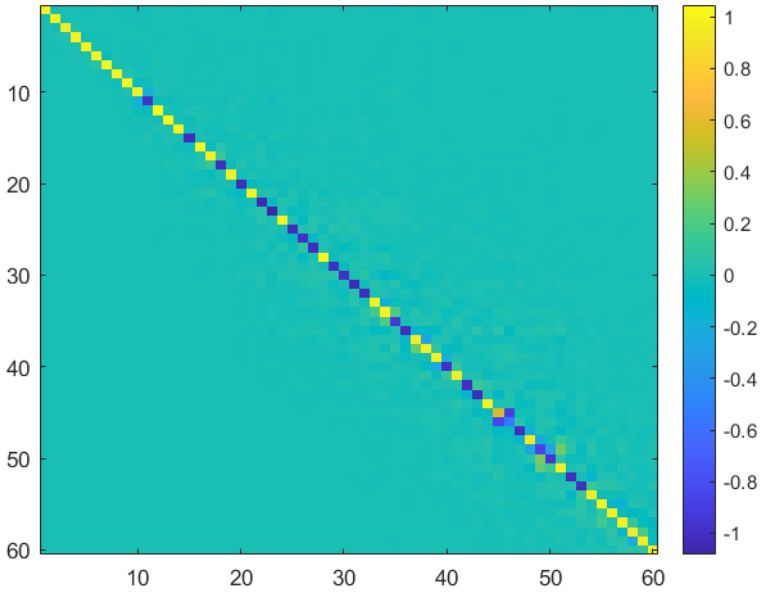

Figure 3.6: Matrix C of size 60×60

3.3.4 Conversion to Point-to-Point Map

Now I have a functional matrix C of size $k \times k$ that encodes the transformation from the functional space of N to that of M; but I need to return to a point-to-point mapping (figure 3.7) to evaluate how the thickness function is trasferred from the source shape M to the target shape N.
Given a matrix Φ^M of the Laplace-Beltrami eigenfunctions of M, where each column corresponds to a point and each row to an eigenfunction, I can find the image of all the functions centered at points of M simply as $C\Phi^M$. Therefore an efficient way to find correspondences between

points is to consider for every point of $C\Phi^M$ its nearest neighbor in Φ^N. To obtain this, I decided to use the K-Nearest Neighbors algorithm.

$$pC = KNN(C\Phi^M, \Phi^N) \tag{3.12}$$

finds the nearest neighbor in Φ^M for each query point in Φ^N and returns the indices of the nearest neighbors in a column vector. These column vector has the same number of rows as Φ^N.

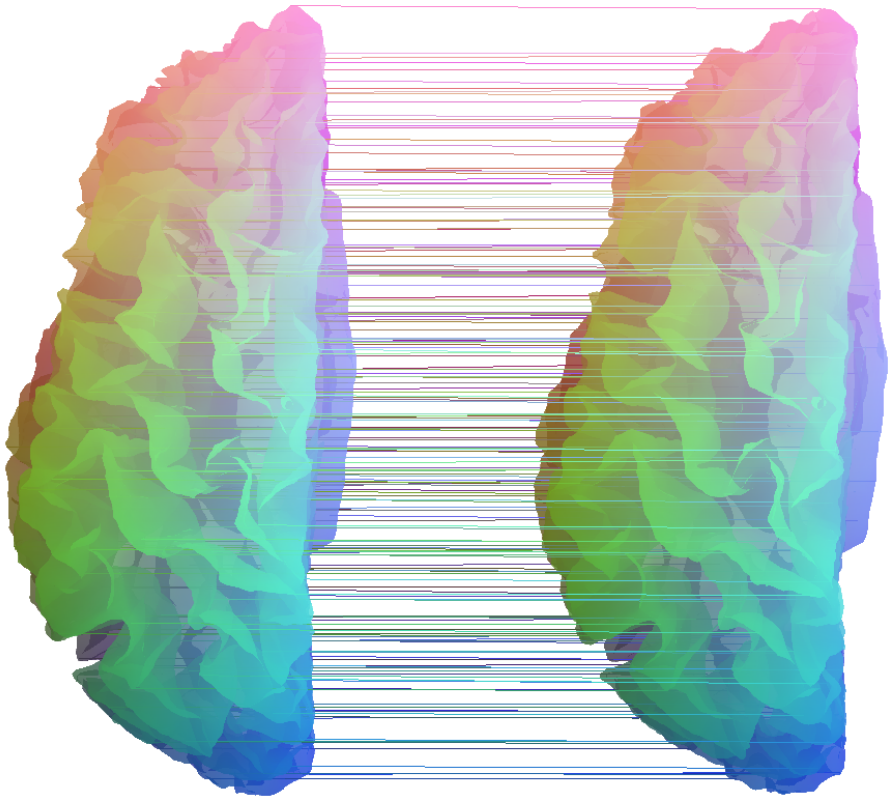

Figure 3.7: Point-to-point mapping obtained by equation (3.12)

3.3.5 Evaluation of Thickness

The goal is to distinguish healthy patients from those presenting the first symptoms of the disease. As described in chapter 2, one of the symptoms of Huntington's disease is the death of some neurons in the brain and the consequent atrophy of the brain organ. By cerebral atrophy we mean the reduction of brain tissue, consequent to the necrosis and shrinkage of the cells that make up the aforementioned tissue. Brain atrophy involves a loss of the functions performed by the brain. The extent of this loss depends on the extent of the brain areas affected by the processes of cell necrosis and shrinkage and it is possible to perceive

Algorithm 3 Functional Maps

Input : Source shape M, target shape N

Output : Functional matrix C

Choice $\phi_i^M \in \mathbb{R}^{|M|\times i}$ and $\phi_j^N \in \mathbb{R}^{|N|\times j}$ // Compute the first i Laplace-Beltrami eigenfunctions of M and the first j Laplace-Beltrami eigenfunctions of N.

Select $\phi_k^M \in \mathbb{R}^{|M|\times k}$ and $\phi_k^N \in \mathbb{R}^{|N|\times k}$ // The first k Laplace-Beltrami eigenfunctions of M and the first k Laplace-Beltrami eigenfunctions of N.

Choose $l_x^M \in M$ and $l_x^N \in N$ // Select x landmark on M and x landmarks on N

$[Fct_x^M, Fct_x^N] \longleftarrow WKS(l_x^M, l_x^N, \phi_k^M, \phi_k^N)$ // Compute descriptors as the average probabilities of qantum particles of different energy levels to be measured in l_x^M on M and in l_x^N on N.

$C \leftarrow \min_P \sum_x \| PFct_x^N - Fct_x^M \|_F^2 + \alpha \sum_k \| \phi_k^M P - P\phi_k^N \|_F^2$ // Minimization problem for C resulting in a matrix of size $k \times k$ and that encodes $C : \mathcal{F}(N, \mathbb{R}) \to \mathcal{F}(M, \mathbb{R})$.

$pC \leftarrow KNN(C\Phi^M, \Phi^N)$ // find the point-to-point map pC with K-Nearest Neighbors algorithm, where Φ^M and Φ^N are the matrices of the Laplace-Beltrami eigenfunctions of M and N

differences between a healthy patient and a sick patient from the loss of volume mainly caused by thinning.
Consequently, given four visits, V_1, V_2, V_3, V_4, which represent the visits at time $t = 1, 2, 3, 4$; , we found the point-to-point correspondences between the pairs (V_1, V_2), (V_1, V_3), (V_1, V_4). So, the point-to-point mapping has changed according to the degeneration / non-degeneration of the patient's brain and consequently will transfer the thickness function more or less precisely.
It will then be possible to analyze the difference in thickness between the various (V_1, V_2), (V_1, V_3), (V_1, V_4) pairs and verify whether this reduction is accentuated in the case of a patient in which the first symptoms of disease begin to arise compared to healthy patients.
At this point I find a point-to-point correspondence between the original shape and the target shape. Thanks to the use of Freesurfer, in addition to extrapolating the surfaces of the hemispheres of the brain, it was possible to obtain a thickness value for each point belonging to the source and the target shapes. These values can represent a Th^M function on shape M and a Th^N function on shape N. Through the point-to-point correspondence obtained, it is therefore possible to transfer the values of the Th^M function on the target shape N, thus obtaining a $Th^{M\to N}$ vector.

What we want to do is see if it is possible to get a better registration of the brains using the functional map extracted thanks to the Functional Maps algorithm, instead of using the global registration made by Freesurfer. In the best case, i.e. in which the patient is healthy, cellular degeneration should be minimal and therefore the difference

$$\Delta th = Th^{M \to N} - Th^{N} \tag{3.13}$$

between $Th^{M \to N}$ and Th^{N} should tend to very low values. On the other hand, if a patient already presents even mild symptoms of Huntington's disease, as the mapping would be less precise, Δth would reach higher values allowing us to distinguish in this way healthy and sick patients.

Chapter 4

Dataset

In this chapter I will show the dataset on which the two methods presented in the previous chapter (3) were performed. In particular, section 4.1 will describe what the dataset contains, while section 4.2 will explain how these data have been filtered, tuned and extracted to be used later.

4.1 Dataset Composition

As mentioned above, I had both a transversal and a longitudinal study available. The dataset is made up of 85 total patients, divided into 44 presymptomatic patients (*earlyHD*) and 41 healthy patients (*control*). For each *earlyHD*, 4 visits are available, carried out approximately one year from one to the other. As for the *control* patients, 7 visits are available at the same time distance. Of these patients, 48 are female, while the remaining 37 are male. Other data are collected in the table 4.1.

	control			**earlyHD**		
	Number	Mean Age	Std Age	Number	Mean Age	Std Age
female	23	46.3	10.9	25	48.6	10.3
male	18	42.8	8.4	19	45.2	9.4

Table 4.1: Dataset description

4.2 How Data Was Preprocessed

From the dataset, thanks to the use of Freesurfer, I first obtained a volumetric reconstruction of the patients' brains, from which I then extracted the white surface and calculated the thickness as the difference between the white surface and the pial surface. In order to use and process this data I have coded the white surface in an .ASC file organized as follows: the first row contains the total number of points and the number of triangular faces that make up the shape of the white surface; each subsequent line indicates a point on the surface and contains its coordinates on a three-dimensional plane (figure 4.1); after the list of all points, triplets of three numbers are listed. Each trio indicates a face and which points constitute it (figure 4.2). Each hemisphere of the brain has a variable number of points and consequently also of faces, but all of them are between 138,000 and 144,000 points and 283,000 and 288,000 faces. Thanks to this file, I was then able to reconstruct the meshes of the brain hemispheres necessary to be able to apply the Functional Maps algorithm.
As for the thickness, the procedure is similar but in this case the corresponding thickness value is indicated next to the coordinates of a point (figure 4.3).

```
ASC
142458 284912
-4.983787  -69.089851  -26.384542  0
-5.550297  -69.024002  -26.528465  0
-6.351344  -68.868599  -26.835215  0
-6.831553  -68.823845  -26.851894  0
-4.891927  -69.152512  -27.130930  0
-5.658632  -69.093208  -27.259260  0
-6.104407  -68.973801  -27.578112  0
-6.856150  -68.869972  -27.337278  0
-3.430480  -68.891930  -28.588556  0
-4.174754  -69.267036  -28.182734  0
-5.449632  -69.348770  -28.173008  0
-6.380630  -68.933449  -28.159914  0
-7.194897  -68.786995  -28.130207  0
-7.545774  -68.694115  -28.648932  0
-3.821608  -69.144051  -29.124891  0
-4.740334  -69.292053  -29.277719  0
-5.553352  -69.094414  -29.082064  0
-6.034105  -68.944771  -28.741211  0
-6.874413  -68.901329  -28.927010  0
-7.654067  -68.697784  -29.344992  0
-3.963259  -68.950287  -30.130716  0
-4.843074  -69.129272  -30.271694  0
-5.494717  -68.962868  -29.878012  0
-6.208301  -68.888069  -29.472256  0
-7.028276  -68.898972  -29.903414  0
-7.810631  -68.640785  -30.330530  0
-3.709599  -68.703934  -31.081951  0
-4.534042  -69.072083  -31.193310  0
-5.519758  -69.061920  -30.827065  0
-6.300655  -68.856400  -30.383656  0
-7.141030  -68.682693  -30.884893  0
-7.660541  -68.613014  -30.901577  0
-4.690616  -68.909904  -32.117939  0
-5.483053  -68.926567  -31.776646  0
-6.421219  -68.711655  -31.318842  0
-6.950500  -68.618706  -31.305662  0
-5.636270  -67.926331  -25.018206  0
-6.259904  -67.999382  -24.955734  0
-7.146766  -68.030823  -25.002464  0
-8.063354  -67.899071  -25.261662  0
```

Figure 4.1: First part of file .ASC that describes the white surface

```
234934   45782 47196 47195 0
234935   45783 45799 47209 0
234936   45783 47209 47196 0
234937   45784 47197 47211 0
234938   45784 47211 45800 0
234939   45786 45787 47200 0
234940   45786 47200 47199 0
234941   45787 45802 45803 0
234942   45787 45803 45788 0
234943   45787 45788 47201 0
234944   45787 47201 47200 0
234945   45788 45803 47214 0
234946   45788 47214 47201 0
234947   45789 45790 47204 0
234948   45789 47204 47203 0
234949   45789 47203 47219 0
234950   45789 47219 45807 0
234951   45791 47205 45792 0
234952   47206 45792 47205 0
234953   45791 45809 47222 0
234954   45791 47222 47205 0
234955   45795 45796 45811 0
234956   45795 45811 45810 0
234957   45795 47207 45796 0
234958   47208 45796 47207 0
234959   45796 47208 45811 0
234960   47223 45811 47208 0
234961   45799 45813 47225 0
234962   45799 47225 47209 0
234963   45800 45801 45816 0
234964   45800 45816 45815 0
234965   45800 47211 45801 0
234966   47212 45801 47211 0
234967   45801 47212 45816 0
234968   47228 45816 47212 0
234969   45803 45804 47215 0
234970   45803 47215 47214 0
234971   45804 45817 45805 0
234972   45818 45805 45817 0
234973   45804 45805 47216 0
```

Figure 4.2: Second part of file .ASC that describes the white surface

```
ASC
000 -12.90976 -76.70282 -5.08028 2.28321
001 -13.15858 -76.75529 -5.24489 2.22987
002 -7.63500 -76.93151 -6.05766 1.94218
003 -7.87122 -76.92839 -6.01651 2.04140
004 -12.82368 -76.91016 -5.66822 2.22642
005 -13.45221 -76.83788 -5.68569 2.19800
006 -13.78818 -76.88177 -6.15057 2.18953
007 -6.79510 -77.02191 -7.11217 1.94128
008 -7.25106 -77.05135 -6.59583 1.95514
009 -7.95696 -77.10114 -6.45772 2.14323
010 -8.69820 -77.16167 -6.79018 2.17913
011 -12.89962 -77.12358 -6.63037 1.93011
012 -13.32017 -77.14738 -6.30865 2.06296
013 -13.76378 -77.08805 -6.66047 2.01941
014 -6.60010 -77.09864 -7.50483 1.95761
015 -7.28082 -77.24802 -7.45985 2.10767
016 -8.28466 -77.33079 -7.42119 2.07693
017 -8.79429 -77.25437 -7.53083 2.06463
018 -12.97528 -77.19729 -7.15291 1.76969
019 -13.39261 -77.25055 -7.04499 1.83667
020 -14.03378 -77.08868 -7.24149 1.85310
021 -4.81867 -76.95814 -8.89588 1.74568
022 -5.53478 -77.19293 -8.70209 1.91693
023 -6.24542 -77.18095 -8.05987 1.91004
024 -7.06768 -77.38482 -8.41939 2.07380
025 -7.97888 -77.41398 -8.26662 2.05053
026 -8.59900 -77.35674 -7.99466 2.05055
027 -13.17801 -77.15691 -7.59255 1.65858
028 -13.76249 -77.15061 -7.60929 1.70339
029 -14.04850 -77.09339 -7.62420 1.74409
030 -4.36280 -77.07959 -9.48581 1.83884
031 -5.05692 -77.19357 -9.41078 2.05450
032 -6.25314 -77.33830 -9.29701 2.02229
033 -7.50774 -77.36237 -9.03521 1.98255
034 -8.14677 -77.30431 -8.86078 2.02473
035 -2.02253 -76.86861 -10.69225 2.11919
036 -2.61378 -76.91385 -10.44389 2.03049
037 -3.34221 -77.17706 -10.34399 2.05607
038 -4.30209 -77.28291 -10.11395 2.09382
039 -5.33340 -77.25036 -10.16953 2.00936
040 -6.07538 -77.24888 -10.14030 1.84629
```

Figure 4.3: File .ASC that describes thickness

Chapter 5

Results Analysis

In this chapter, I will present the results obtained from the two methods explained in chapter 3, dividing the analysis into two sections. The sections will be dedicated respectively to the two methods used where I will also show the process chosen for the evaluation of the results. In particular, the results are validated by the use of two statistical tests: the Kruskal-Wallis test and the Wilcoxon Rank Sum test, explained in detail in the first section.

5.1 Freesurfer Data Analysis

I had both a cross-sectional study (visits of different patients) and a longitudinal study (visits of the same patient after a certain period of time, equivalent to about one year). In this way it was possible to extract the values of the cortical thickness both for different patients and for the same patient for different years. From the analysis of these data, the goal was to try to be able to classify healthy patients (*control*) from those affected by the first symptoms of Huntington's disease (*earlyHD*) thanks to a study on the patients' cortical thickness.
As explained in chapter 3, through the formula 3.5 the goal is to highlight a statistically evident degeneration of thickness in *earlyHD* patients, compared to *control* patients. As mentioned in chapter 4, the brain of each patient is analyzed separately in the right and left hemisphere as can be seen in figures 5.1 and in figure 5.2. Figure 5.3 instead combines in a single graph the results obtained on the two hemispheres. In the last figure (5.4), I plot, for each time instant, the average of the values.

5.1.1 Kruskal-Wallis test

In Statistics, the Kruskal-Wallis test ([24]) is a non-parametric method to verify the equality of the medians of different groups; that is, to verify

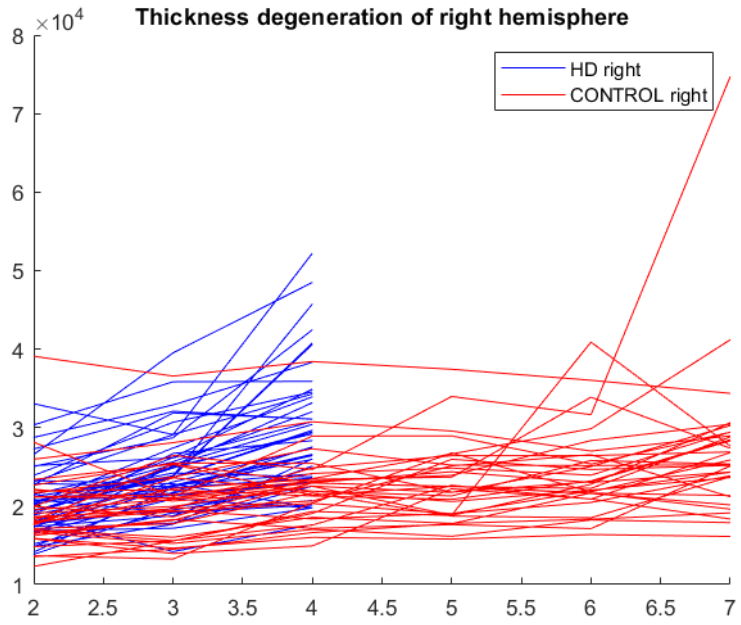

Figure 5.1: Freesurfer Data Analysis: results obtained on the right hemispheres of patients. Each blue broken line indicates an earlyHD patient, while the red ones indicate control patients. The line is obtained by joining the values obtained through equation 3.1, calculated for each time instant. Time instants, ranging in the interval [2,7], are indicated on the horizontal axis, while the total value of the decrease in thickness with respect to the time instant $t = 1$ (the first available visit) are indicated on the vertical axix.

that these groups come from the same population (or from populations with the same median). It is named after its authors William Kruskal and W. Allen Wallis. This method is the non-parametric correspondent of the analysis of variance where data is replaced by their rank, and is usually used when a normal population distribution cannot be assumed. Using this statistical test, the goal is to demonstrate that the "behavior" of the cortical thickness of a healthy patient (*control*) differs from that of a presymptomatic patient (*earlyHD*).
Specifically, I test:

- Null hypothesis: which states that the set of values calculated through equation 3.5 on healthy patients (*control*) and the set of values calculated on presymptomatic patients (*earlyHD*) come from the same distribution with the same median, which means that the values tested are attributable to a single group. We expect to reject this hypothesis, as we believe that the behavior between the two groups clearly diverges.

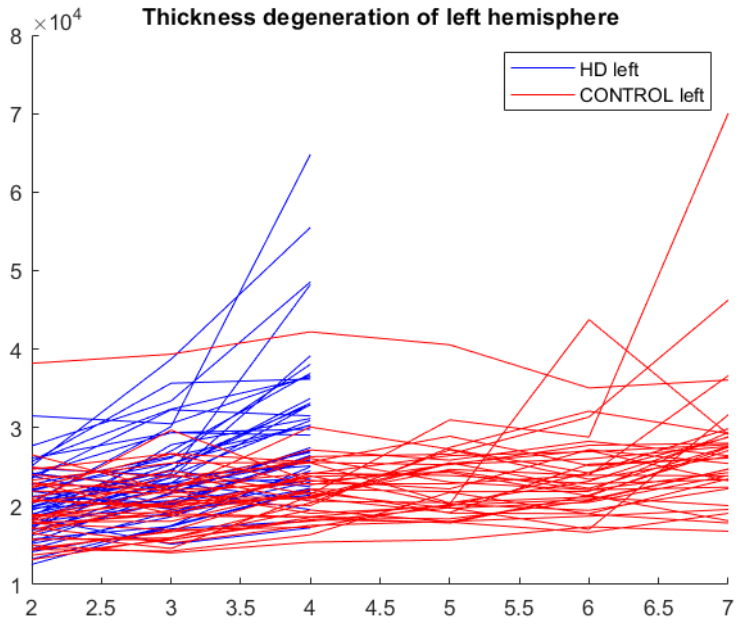

Figure 5.2: Freesurfer Data Analysis: results obtained on the left hemispheres of patients. Each blue broken line indicates an earlyHD patient, while the red ones indicate control patients. The line is obtained by joining the values obtained through equation 3.5, calculated for each time instant. Time instants, ranging in the interval [2,7], are indicated on the horizontal axis, while the total value of the decrease in thickness with respect to the time instant $t = 1$ (the first available visit) are indicated on the vertical axix.

- Alternative hypothesis: which states that the set of values calculated through equation 3.5 on healthy patients (*control*) and the set of values calculated on presymptomatic patients (*earlyHD*) come from different distributions with different medians, which means that the tested values are attributable to two separate groups. We expect to accept this hypothesis because it would prove statistical evidence that the decrease in cortical thickness is attributable to the onset of Huntington's disease.

For the test I used a significance level of 5%. The analysis, which I run with these tests, returns a p-value. If the p-value reaches and exceeds a value of 0.05 then the null hypothesis is accepted, otherwise it will be discarded and the alternative hypothesis accepted. The lower the p-value is, the higher is the evidence of the different distribution of the analyzed groups.
The problem with this statistical test is that the samples must be the same length. Therefore, only the time interval [1,4] was considered even if the interval available for control patients was [1,7].

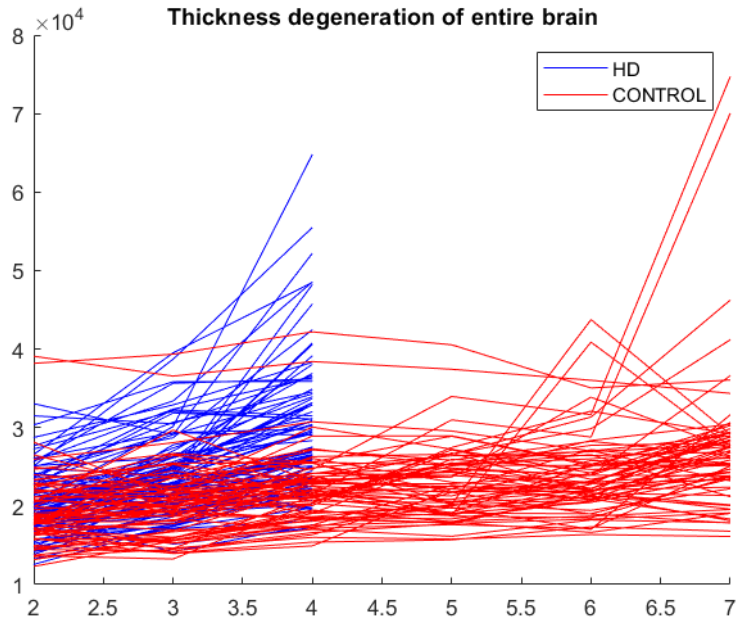

Figure 5.3: Freesurfer Data Analysis: results obtained on the whole brain of patients. Each blue broken line indicates an earlyHD patient, while the red ones indicate control patients. The line is obtained by joining the values obtained through equation 3.1, calculated for each time instant. Time instants, ranging in the interval [2,7], are indicated on the horizontal axis, while the total value of the decrease in thickness with respect to the time instant $t = 1$ (the first available visit) are indicated on the vertical axix.

The Kruskal-Wallis test was performed on both the right and left hemisphere and the entire brain of the patients. The results obtained are shown in figures 5.5, 5.6, 5.7. In all three tests the null hypothesis was rejected. This means that the method used was able to achieve its goal, which is to distinguish *control* patients and *earlyHD* patients.

It is possible to extend the analysis by performing a multiple comparison test using the information obtained from the Kruskal-Wallis test which allows to return a matrix of pairwise comparison results. Each row of the matrix represents a test and there is a row for each pair of groups. The items in the row indicate the compared means, the estimated difference in the means, and a confidence interval for the difference.
A graphic representation of the test is shown in figure 5.8.

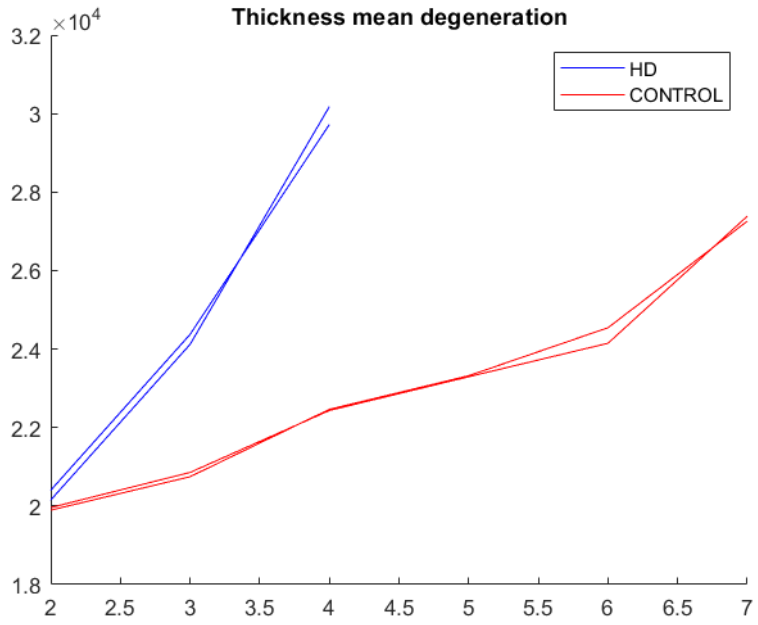

Figure 5.4: Freesurfer Data Analysis: this plot shows the average of the results for each hemisphere of the brain. Time instants, ranging in the interval [2,7], are indicated on the horizontal axis, while the average of the total value of the decrease in thickness with respect to the time instant $t = 1$ (the first available visit) is indicated on the vertical axix.

5.1.2 Wilcoxon Rank Sum Test

The Wilcoxon rank sum test ([25]) is a nonparametric test for two populations when samples are independent. If X and Y are independent samples with different sample sizes, the test statistic returns the rank sum of the first sample. The Wilcoxon rank sum test is equivalent to the Mann-Whitney U-test. The Mann-Whitney U-test is a nonparametric test for equality of population medians of two independent samples X and Y.
In my case, I used the two-sided Wilcoxon rank sum test to demonstrate that the "behavior" of the cortical thickness of a healthy patient (*control*) differs from that of a presymptomatic patient (*earlyHD*). A substantial difference to note is that this test does not work by comparing groups of samples (such as Kruskal-Wallis test) but compares only two samples. In order to use this method I have therefore created two vectors: the first contains all the values calculated on the *control* patients while the second contains all the values calculated on the *earlyHD* patients. The advantage of this test compared to the previous one, however, is that here the samples can have different lengths allowing me to use the

calculated data along the entire time interval.
In particular, I test:

- Null hypothesis: which states that the set of values calculated through equation 3.5 on healthy patients (*control*) and the set of values calculated on presymptomatic patients (*earlyHD*) are samples from continuous distributions with equal medians. We expect to reject this hypothesis, as we believe that the behavior between the two samples clearly diverges.

- Alternative hypothesis: which states that the set of values calculated through equation 3.5 on healthy patients (*control*) and the set of values calculated on presymptomatic patients (*earlyHD*) come from different distributions with different medians, which means that the tested values are attributable to two separate samples. We expect to accept this hypothesis because it would prove statistical evidence that the decrease in cortical thickness is attributable to the onset of Huntington's disease.

For the test I used a significance level of 5%. The analysis, which I run with these tests, returns a p-value. If the p-value reaches and exceeds a value of 0.05 then the null hypothesis is accepted, otherwise it will be discarded and the alternative hypothesis accepted. The lower the p-value is, the higher is the evidence of the different distribution of the analyzed groups.
The Wilcoxon Rank Sum Test was performed on both the right and left hemisphere and the entire brain of the patients.
Another alternative hypothesis was also tested. Instead of verifying that the two samples have different medians, it is tested if the median of the data concerning *control* patients is lower than that concerning *earlyHD* patients. The results obtained are shown in table 5.1 and 5.2.

	P-value	**Result of the Hypothesis test**
right hemisphere	0.0251	Null Hypothesis Rejected
left hemisphere	0.0426	Null Hypothesis Rejected
entire brain	0.0026	Null Hypothesis Rejected

Table 5.1: Freesurfer Data Analysis: Wilcoxon rank sum test. Null hypothesis of equal medians.

Another experiment performed was to try to compare the degeneration of thickness in the brains of *control* patients compared to *earlyHD* patients, not using all the available visits but progressively reducing this

	P-value	Result of the Hypothesis test
right hemisphere	0.0125	Null Hypothesis Rejected
left hemisphere	0.0213	Null Hypothesis Rejected
entire brain	0.0013	Null Hypothesis Rejected

Table 5.2: Freesurfer Data Analysis: Wilcoxon rank sum test. Alternative hypothesis is that the median of control patients is lower than the median of earlyHD patients.

number to verify until I was able to reject the null hypothesis of the test. Tables 5.3, 5.4, 5.5 summarize the results obtained on different time interval for the right, left or entire brain of the patients respectively. As can be deduced from the results reported, the null hypothesis is accepted only considering the time interval [1,2], i.e. taking into account only one visit after the first one. In the rest of the cases, however, it appears statistically evident that healthy patients and sick patients have two different distributions, with different medians.

Time Interval	P-value	Result of the Hypothesis test
[1,4]	$3.43e^{-6}$	Null Hypothesis Rejected
[1,3]	0.0043	Null Hypothesis Rejected
[1,2]	0.4844	Null Hypothesis Accepted

Table 5.3: Freesurfer Data Analysis: Wilcoxon rank sum test on different time interval on the right hemisphere of the brain.

Time Interval	P-value	Result of the Hypothesis test
[1,4]	$1.608e^{-6}$	Null Hypothesis Rejected
[1,3]	0.0169	Null Hypothesis Rejected
[1,2]	0.6761	Null Hypothesis Accepted

Table 5.4: Freesurfer Data Analysis: Wilcoxon rank sum test on different time interval on the left hemisphere of the brain.

Time Interval	P-value	Result of the Hypothesis test
[1,4]	$2.453e^{-10}$	Null Hypothesis Rejected
[1,3]	$1.962e^{-4}$	Null Hypothesis Rejected
[1,2]	0.4328	Null Hypothesis Accepted

Table 5.5: Freesurfer Data Analysis: Wilcoxon rank sum test on different time interval on the entire brain.

5.2 Functional Maps Data Analysis

As for the previous method, the goal is to be able to classify (*control*) patients from those (*earlyHD*) thanks to a study on the patients' cortical thickness. As explained in chapter 3, through the formula 3.13 the goal is to highlight a statistically evident degeneration of thickness in *earlyHD* patients, compared to *control* patients.
As for the first method, the analysis is made on right (figure 5.9) and left hemisphere (figure 5.10) and on the entire brain of the patients (figure 5.11). In the last figure (5.12), I plot, for each time instant, the average of the values.

5.2.1 Kruskal-Wallis test

As for the previous method, I used the Kruskal-Wallis test to demonstrate that the "behavior" of the cortical thickness of a healthy patient (*control*) differs from that of a presymptomatic patient (*earlyHD*). For the test I used a significance level of 5%. The analysis, which I run with these tests, returns a p-value. If the p-value reaches and exceeds a value of 0.05 then the null hypothesis is accepted, otherwise it will be discarded and the alternative hypothesis accepted. The Kruskal-Wallis test was performed on both the right and left hemisphere and the entire brain of the patients. The results obtained are shown in figures 5.13, 5.14, 5.15. In all three tests the null hypothesis was rejected. This means that the method used was able to achieve its goal, which is to distinguish control patients and earlyHD patients.

I extend the analysis by performing a multiple comparison test using the information obtained from the Kruskal-Wallis test; a graphic representation of the test is shown in figure 5.16.

5.2.2 Wilcoxon Rank Sum Test

Also for this second metheod, I used the two-sided Wilcoxon rank sum test to test the results. I used a significance level of 5%. If the p-value

reaches and exceeds a value of 0.05 then the null hypothesis is accepted, otherwise it will be discarded and the alternative hypothesis accepted. The Wilcoxon Rank Sum Test was performed on both the right and left hemisphere and the entire brain of the patients.
The results obtained are shown in table 5.6 and 5.7.

	P-value	**Result of the Hypothesis test**
right hemisphere	0.0064	Null Hypothesis Rejected
left hemisphere	0.0026	Null Hypothesis Rejected
entire brain	$3.6e^{-5}$	Null Hypothesis Rejected

Table 5.6: Functional Maps Data Analysis: Wilcoxon rank sum test. Null hypothesis of equal medians.

	P-value	**Result of the Hypothesis test**
right hemisphere	0.0032	Null Hypothesis Rejected
left hemisphere	0.0013	Null Hypothesis Rejected
entire brain	$1.8e^{-5}$	Null Hypothesis Rejected

Table 5.7: Functional Maps Data Analysis: Wilcoxon rank sum test. Alternative hypothesis is that the median of control patients is lower than the median of earlyHD patients.

The same experiment performed in the first method tries to compare the degeneration of thickness in the brains of *control* patients compared to *earlyHD* patients, not using all the available visits but progressively reducing this number to verify until I was able to reject the null hypothesis of the test. Tables 5.8, 5.9, 5.10 summarize the results obtained on different time interval for the right, left or entire brain of the patients respectively. As can be deduced from the results reported, the null hypothesis is accepted only considering the time interval [1,2], i.e. taking into account only one visit after the first one. In the rest of the cases, however, it appears statistically evident that healthy patients and sick patients have two different distributions, with different medians. Even with this method I therefore achieve the set goal, that is to be able to identify Huntington's patients at a presymptomatic stage.

Time Interval	P-value	Result of the Hypothesis test
[1,4]	$1.015e^{-5}$	Null Hypothesis Rejected
[1,3]	0.0030	Null Hypothesis Rejected
[1,2]	0.2655	Null Hypothesis Accepted

Table 5.8: Functional Maps Data Analysis: Wilcoxon rank sum test on different time interval on the right hemisphere of the brain.

Time Interval	P-value	Result of the Hypothesis test
[1,4]	$2.284e^{-6}$	Null Hypothesis Rejected
[1,3]	0.0025	Null Hypothesis Rejected
[1,2]	0.1561	Null Hypothesis Accepted

Table 5.9: Functional Maps Data Analysis: Wilcoxon rank sum test on different time interval on the left hemisphere of the brain.

Time Interval	P-value	Result of the Hypothesis test
[1,4]	$7.118e^{-11}$	Null Hypothesis Rejected
[1,3]	$1.895e^{-5}$	Null Hypothesis Rejected
[1,2]	0.0677	Null Hypothesis Accepted

Table 5.10: Functional Maps Data Analysis: Wilcoxon rank sum test on different time interval on the entire brain.

Kruskal-Wallis ANOVA Table

Source	SS	df	MS	Chi-sq	Prob>Chi-sq
Groups	117311.4	1	117311.4	21.56	3.42108e-06
Error	1264448.6	253	4997.8		
Total	1381760	254			

(a) Kruskal-Wallis ANOVA table

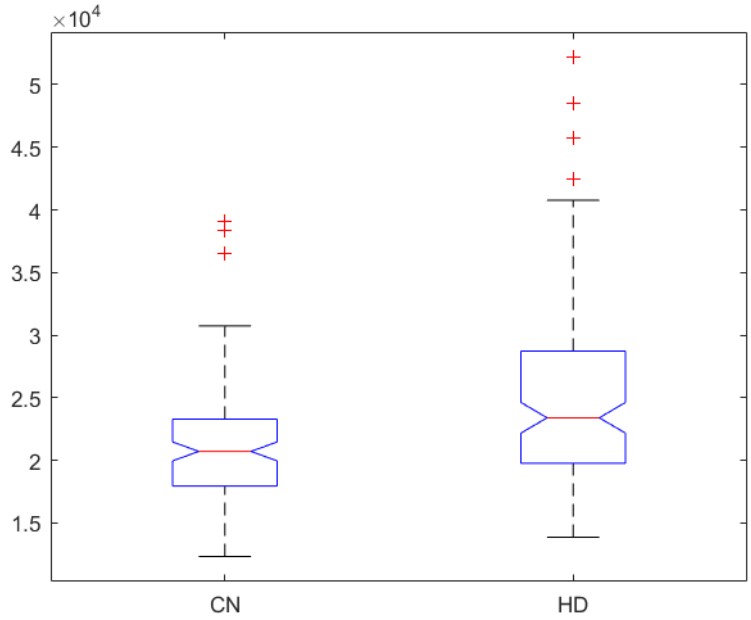

(b) Kruskal-Wallis boxplot. CN stands for *control* and HD stands for *earlyHD*

Figure 5.5: Freesurfer Data Analysis: results of Kruskal-Wallis test on the right hemisphere of patients. P-value is equal to $3.421e^{-6}$. The returned p-value indicates that Kruskal-Wallis test rejects the null hypothesis that control and earlyHD come from the same distribution at a 5% significance level. The table (A) provides additional test results, and the boxplot (B) visually presents the summary statistics for each patient in each group.

Kruskal-Wallis ANOVA Table

Source	SS	df	MS	Chi-sq	Prob>Chi-sq
Groups	101248	1	101248	18.61	1.60228e-05
Error	1280511.5	253	5061.3		
Total	1381759.5	254			

(a) Kruskal-Wallis ANOVA table

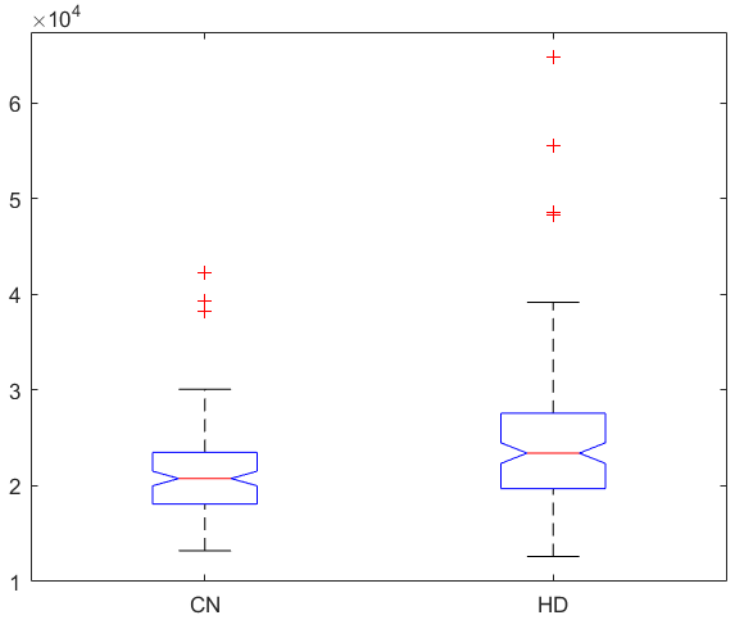

(b) Kruskal-Wallis boxplot. CN stands for *control* and HD stands for *earlyHD*

Figure 5.6: Freesurfer Data Analysis: results of Kruskal-Wallis test on the left hemisphere of patients. P-value is equal to $1.602e^{-5}$. The returned p-value indicates that Kruskal-Wallis test rejects the null hypothesis that control and earlyHD come from the same distribution at a 5% significance level. The table (A) provides additional test results, and the boxplot (B) visually presents the summary statistics for each patient in each group.

Kruskal-Wallis ANOVA Table

Source	SS	df	MS	Chi-sq	Prob>Chi-sq
Groups	938491.6	1	938491.6	43.21	4.90656e-11
Error	10115588.4	508	19912.6		
Total	11054080	509			

(a) Kruskal-Wallis ANOVA table

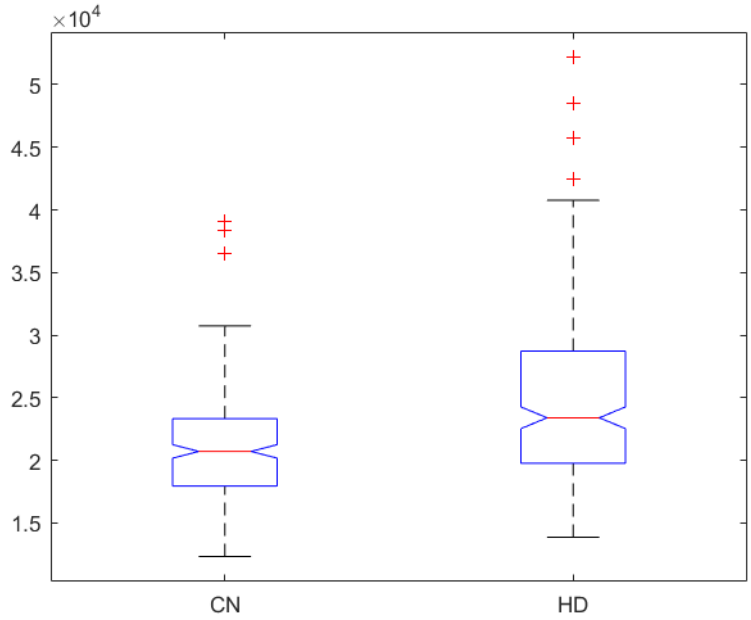

(b) Kruskal-Wallis boxplot. CN stands for *control* and HD stands for *earlyHD*

Figure 5.7: Freesurfer Data Analysis: results of Kruskal-Wallis test on the entire brain of patients.P-value is equal to $4.906e^{-11}$*. The returned p-value indicates that Kruskal-Wallis test rejects the null hypothesis that control and earlyHD come from the same distribution at a 5% significance level. The table (A) provides additional test results, and the boxplot (B) visually presents the summary statistics for each patient in each group.*

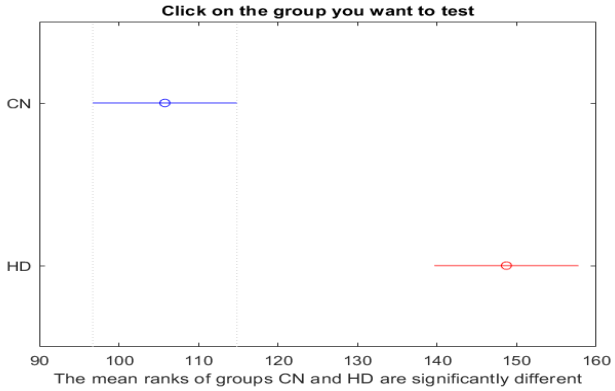

(a) Multiple comparison test of means for right hemisphere

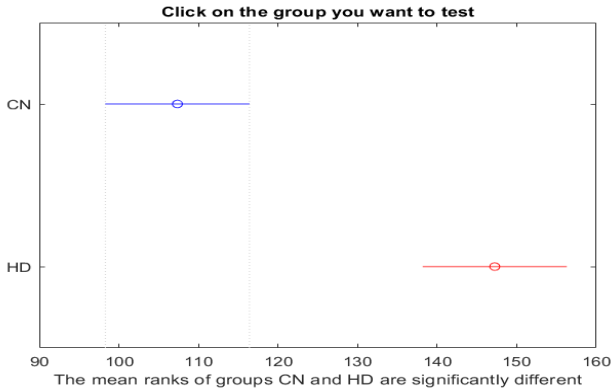

(b) Multiple comparison test of means for left hemisphere

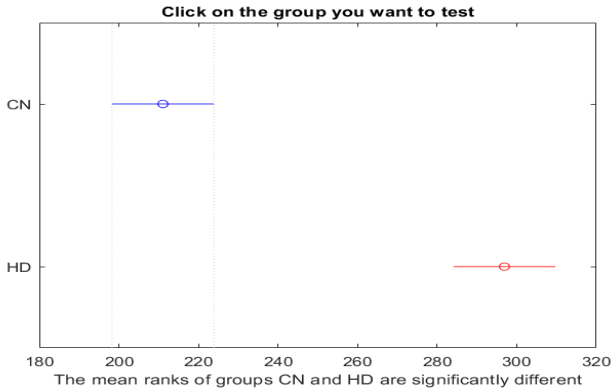

(c) Multiple comparison test of means for the entire brain

Figure 5.8: Freesurfer Data Analysis: multiple comparison test of means. It displays a graph with each group mean represented by a symbol and an interval around the symbol. Two means are significantly different if their intervals are disjoint, and are not significantly different if their intervals overlap.

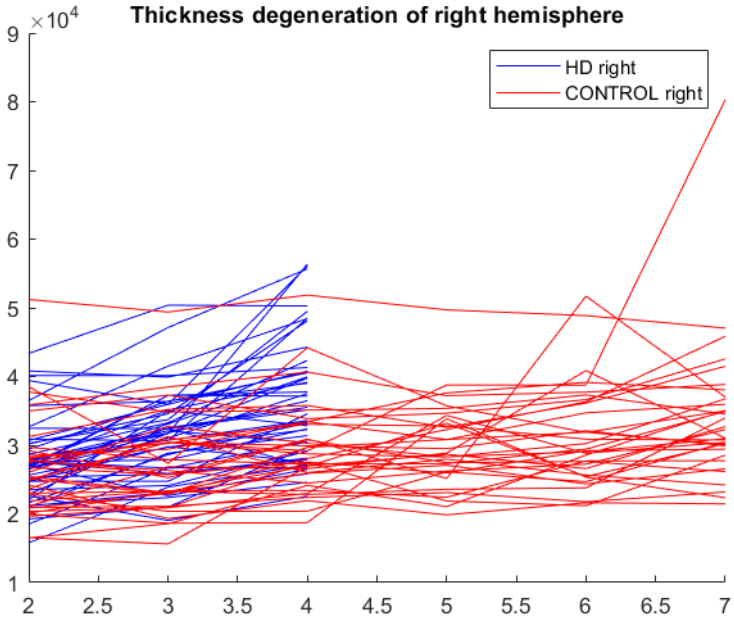

Figure 5.9: Functional Maps Data Analysis: results obtained on the right hemispheres of patients. Each blue broken line indicates an earlyHD patient, while the red ones indicate control patients. The line is obtained by joining the values obtained through equation 3.13, calculated for each time instant. Time instants, ranging in the interval [2,7], are indicated on the horizontal axis, while the total value of the decrease in thickness with respect to the time instant $t = 1$ (the first available visit) are indicated on the vertical axix.

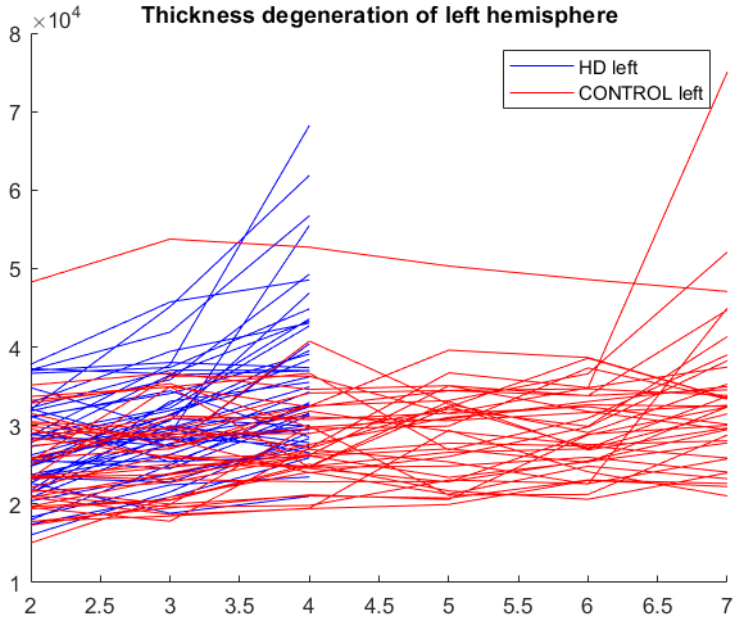

Figure 5.10: Functional Maps Data Analysis: results obtained on the left hemispheres of patients. Each blue broken line indicates an earlyHD patient, while the red ones indicate control patients. The line is obtained by joining the values obtained through equation 3.13, calculated for each time instant. Time instants, ranging in the interval [2,7], are indicated on the horizontal axis, while the total value of the decrease in thickness with respect to the time instant $t = 1$ (the first available visit) are indicated on the vertical axix.

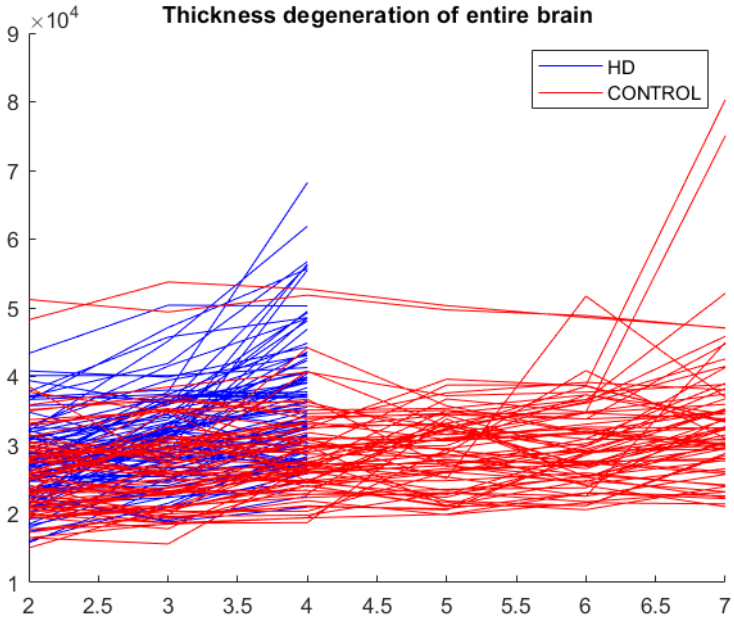

Figure 5.11: Functional Maps Data Analysis: results obtained on the whole brain of patients. Each blue broken line indicates an earlyHD patient, while the red ones indicate control patients. The line is obtained by joining the values obtained through equation 3.9, calculated for each time instant. Time instants, ranging in the interval [2,7], are indicated on the horizontal axis, while the total value of the decrease in thickness with respect to the time instant $t = 1$ (the first available visit) are indicated on the vertical axix.

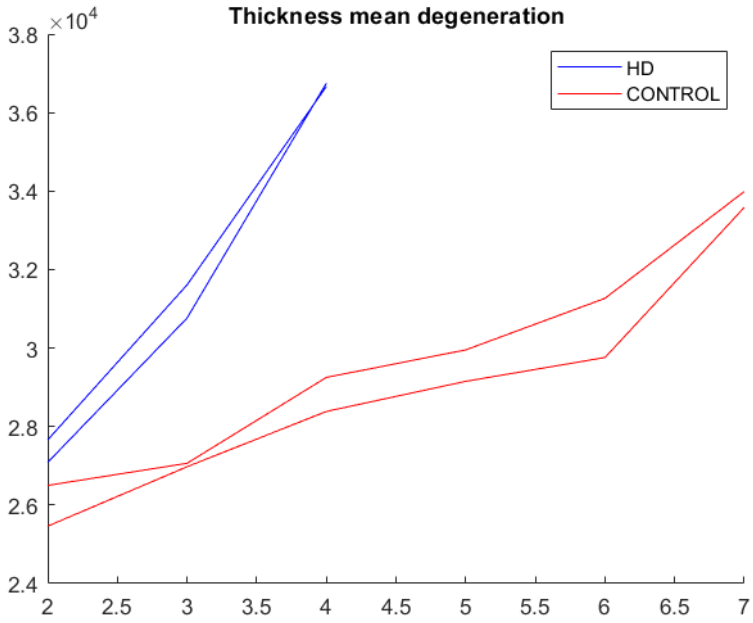

Figure 5.12: Functional Maps Data Analysis: this plot shows the average of the results for each hemisphere of the brain. Time instants, ranging in the interval [2,7], are indicated on the horizontal axis, while the average of the total value of the decrease in thickness with respect to the time instant $t = 1$ (the first available visit) is indicated on the vertical axix.

Kruskal-Wallis ANOVA Table

Source	SS	df	MS	Chi-sq	Prob>Chi-sq
Groups	89319.2	1	89319.2	19.49	1.01055e-05
Error	978403.3	232	4217.3		
Total	1067722.5	233			

(a) Kruskal-Wallis ANOVA table

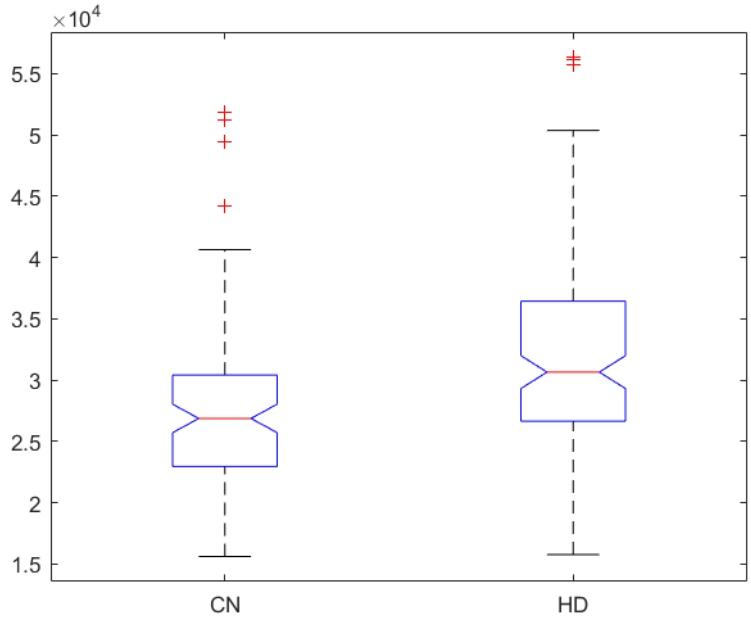

(b) Kruskal-Wallis boxplot. CN stands for *control* and HD stands for *earlyHD*

Figure 5.13: Functional Maps Data Analysis: results of Kruskal-Wallis test on the right hemisphere of patients. P-value is equal to $1.010e^{-5}$. The returned p-value indicates that Kruskal-Wallis test rejects the null hypothesis that control and earlyHD come from the same distribution at a 5% significance level. The table (A) provides additional test results, and the boxplot (B) visually presents the summary statistics for each patient in each group.

Kruskal-Wallis ANOVA Table

Source	SS	df	MS	Chi-sq	Prob>Chi-sq
Groups	113161.3	1	113161.3	22.35	2.27398e-06
Error	1127396.2	244	4620.5		
Total	1240557.5	245			

(a) Kruskal-Wallis ANOVA table

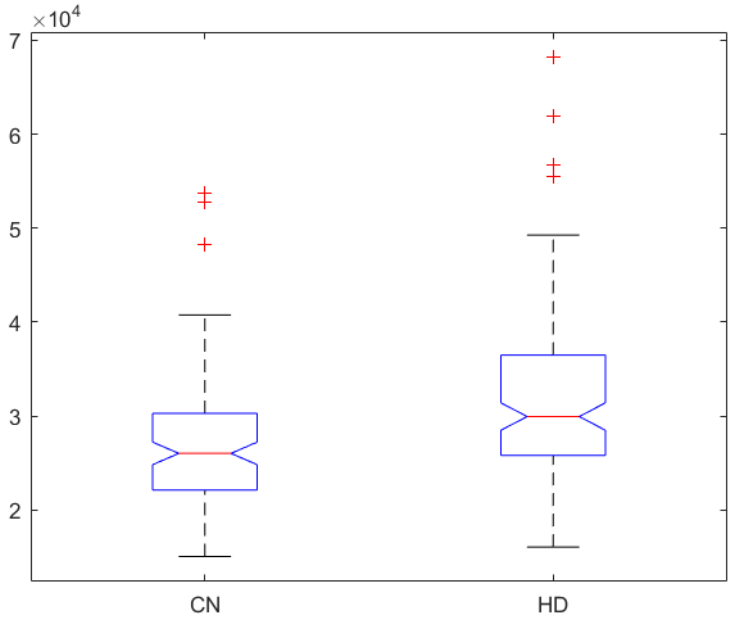

(b) Kruskal-Wallis boxplot. CN stands for *control* and HD stands for *earlyHD*

Figure 5.14: Functional Maps Data Analysis: results of Kruskal-Wallis test on the left hemisphere of patients. P-value is equal to 2.273e^{-6}. The returned p-value indicates that Kruskal-Wallis test rejects the null hypothesis that control and earlyHD come from the same distribution at a 5% significance level. The table (A) provides additional test results, and the boxplot (B) visually presents the summary statistics for each patient in each group.

Kruskal-Wallis ANOVA Table

Source	SS	df	MS	Chi-sq	Prob>Chi-sq
Groups	817517	1	817517	42.49	7.10267e-11
Error	8398443	478	17570		
Total	9215960	479			

(a) Kruskal-Wallis ANOVA table

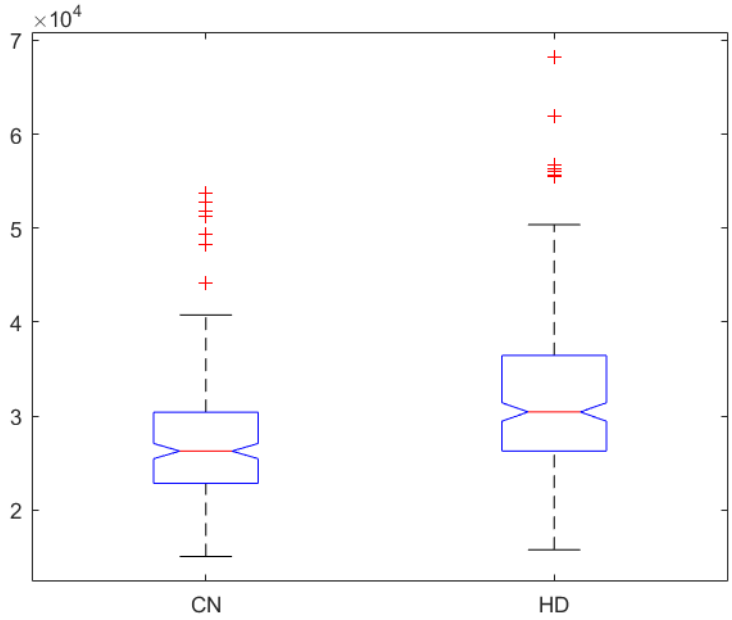

(b) Kruskal-Wallis boxplot. CN stands for *control* and HD stands for *earlyHD*

Figure 5.15: Functional Maps Data Analysis: results of Kruskal-Wallis test on the entire brain of patients.P-value is equal to 7.102e^{-11}. The returned p-value indicates that Kruskal-Wallis test rejects the null hypothesis that control and earlyHD come from the same distribution at a 5% significance level. The table (A) provides additional test results, and the boxplot (B) visually presents the summary statistics for each patient in each group.

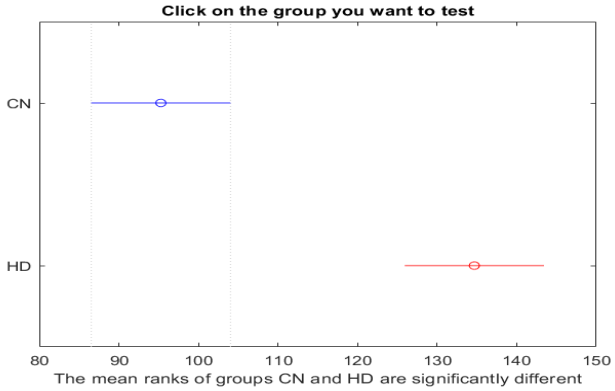

(a) Multiple comparison test of means for right hemisphere

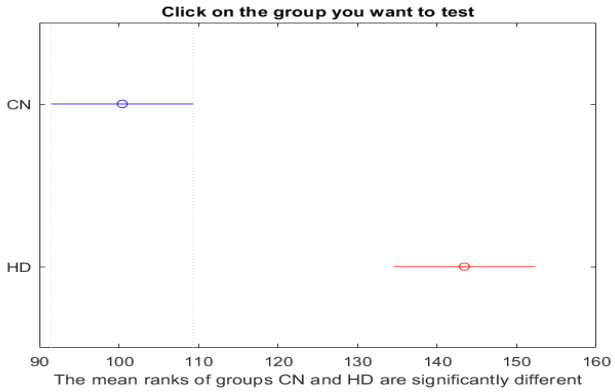

(b) Multiple comparison test of means for left hemisphere

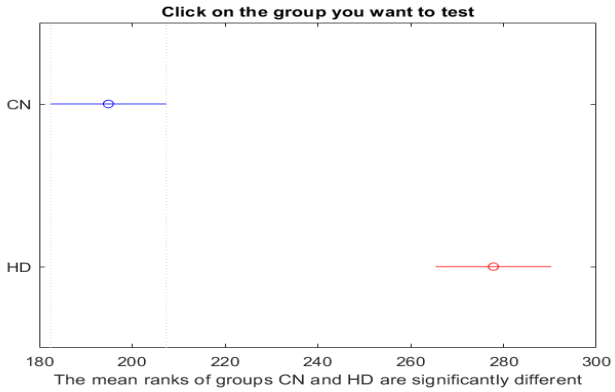

(c) Multiple comparison test of means for the entire brain

Figure 5.16: Functional Maps Data Analysis: multiple comparison test of means. It displays a graph with each group mean represented by a symbol and an interval around the symbol. Two means are significantly different if their intervals are disjoint, and are not significantly different if their intervals overlap.

Chapter 6

Conclusions

The goal of the work is to classify healthy patients (*control*) from those affected by the first symptoms of Huntington's disease (*earlyHD*) thanks to a study on the patients'cortical thickness. In particular, the aim is to highlight whether there is same statistical evidence in degeneration of thickness in *earltyHD* patients, compared to *control* patients.
To achieve this goal, as shown in detail in chapter 3, I used two different methods, one through the use of Freesurfer which allowed to obtain a global registration of the patients' brains, the other, through the use of the algorithm of Functional Maps, which allowed a user-specific registration, directly dependent on the anatomy of the brain of the patient analyzed. Both methods were then validated through the use of two statistical tests, the Kruskal-Wallis test and the Wilcoxon Rank Sum test. As it is evident from the results reported in the previous chapter (5), both methods showed an evident degeneration of the cortical thickness of the brain of patients suffering from Huntington's disease, confirmed by the results of the statistical tests used.
On the one hand, it is possible to use the values of the cortical thickness to identify an *earlyHD* patient, therefore still in the presymptomatic phase. This is a positive result, because succeeding in this means being able to start pharmacological therapies at a very early stage of Huntington's disease, making them much more effective and timely. On the other hand, it is not possible to say that a user-specific brain registration is more effective than a global brain registration since, as it is possible to see in tables 6.1, 6.2, 6.3, the results obtained from the tests are very similar. However, if we evaluate the p-values obtained, it is possible to note that, unlike those obtained with the Kruskal-Wallis test, where the values are of the same order of magnitude, those obtained from the Wilcoxon Rank Sum test on the second method (Functional Maps) have different orders of magnitude, as can be seen in table 6.2. So although both methods reject the null hypothesis which states the distribution equality for *control* and *earlyHD* patients, the lower p-values

of the second method indicate greater evidence. As proof of this, in fact, if the test were conducted with a significance level of 1 % in the cases concerning the right and left hemisphere of the brain, the result would be the acceptance of the null hypothesis as regards the Freesurfer data analysis method, unlike of the Functional Maps data analysis method which would maintain the same results.
It is therefore possible to affirm that even if both methods achieve the intended purpose, the second, in some cases, allows greater precision and therefore greater evidence.
As a final consideration this is one of the few works, together with the one on Brains by S. Melzi et al. [20], that exploits functional maps in the medical field and it also does it successfully.

Kruskal-Wallis	**Freesurfer p-value**	**Functional Maps p-value**
right hemisphere	$3.421e^{-6}$	$1.01e^{-5}$
left hemisphere	$1.602e^{-5}$	$2.273e^{-6}$
entire brain	$4.906e^{-11}$	$7.102e^{-11}$

Table 6.1: Comparison between Kruskal-Wallis test results. Freesurfer: Freesurfer data analysis. Functional Maps: Functional maps data analysis

Wilcoxon rank sum test	**Freesurfer p-value**	**Functional Maps p-value**
right hemisphere	0.0251	0.0064
left hemisphere	0.0426	0.0026
entire brain	0.0026	$3.6e^{-5}$

Table 6.2: Comparison between Wilcoxon rank sum test results. Freesurfer: Freesurfer data analysis. Functional Maps: Functional maps data analysis

Wilcoxon rank sum test		**Freesurfer p-value**	**Functional maps p-value**
right hemisphere	[1,4]	$3.43e^{-6}$	$1.015e^{-5}$
	[1,3]	0.0043	0.0030
	[1,2]	0.4844	0.2655
left hemisphere	[1,4]	$1.608e^{-6}$	$2.284e^{-6}$
	[1,3]	0.0169	0.0025
	[1,2]	0.6761	0.1561
entire brain	[1,4]	$2.453e^{-10}$	$7.118e^{-11}$
	[1,3]	$1.962e^{-4}$	$1.895e^{-5}$
	[1,2]	0.4328	0.0677

Table 6.3: Comparison between Wilcoxon rank sum test results considering different time interval. Freesurfer: Freesurfer data analysis. Functional Maps: Functional maps data analysis

Bibliography

[1] Tamara Pringsheim Katie Wiltshire Lundy Day Jonathan Dykeman Thomas Steeves and Nathalie Jette. "The incidence and prevalence of huntington's disease: A systematic review and meta-analysis". In: *Movement Disorders* (2012).

[2] George Huntington et al. "On chorea". In: (1872).

[3] Sherryl A Taylor Marianne James Nicolet Groot et al. Marcy E MacDonald Christine M Ambrose Mabel P Duyao Richard H Myers Carol Lin Lakshmi Srinidhi Glenn Barnes. "A novel gene containing a trinucleotide repeat that is expanded and unstable on huntington's disease chromosomes". In: (1993).

[4] Walker FO. "Huntington's disease". In: *Lancet* (2007).

[5] Nance MA Myers RH. "Juvenile onset Huntington's disease—clinical and research perspectives". In: *Ment Retard Dev Disabil Res Rev* (2001).

[6] Douglas R Langbehn Jeffrey D Long John H Warner Rachael I Scahill Blair R Leavitt Julie C Stout Jane S Paulsen et al. Christopher A Ross Elizabeth H Aylward Edward J Wild. "Huntington disease: natural history, biomarkers and prospects for therapeutics". In: *Nature Reviews Neurology* (2014).

[7] Karl Kieburtz John B Penney Peter Corno Neal Ranen Ira Shoulson Andrew Feigin Davi Abwender J Timothy Greenarnyre Donald Higgins Frederick J Marshall et al. "Unified huntingtons disease rating scale: reliability and consistency". In: *Neurology* (2001).

[8] Elizabeth H Aylward Peggy C Nopoulos Christopher A Ross Douglas R Langbehn Ronald K Pierson James A Mills Hans J Johnson Vincent A Magnotta Andrew R Juhl Jane S Paulsen et al. "Longitudinal change in regional brain volumes in prodromal huntington disease". In: *Journal of Neurology, Neurosurgery and Psychiatry* (2011).

[9] H Diana Rosas David H Salat Stephanie Y Lee Alexandra K Zaleta Vasanth Pappu Bruce Fischl Doug Greve Nathanael Hevelone and Steven M Hersch. "Cerebral cortex and the clinical expression of huntington's disease: complexity and heterogeneity". In: *Brain* (2008).

[10] E.H. Kim et al. "Chapter 8 - Huntington Disease". In: *The Cerebral Cortex in Neurodegenerative and Neuropsychiatric Disorders*. Ed. by David F. Cechetto and Nina Weishaupt. San Diego: Academic Press, 2017, pp. 195–221. ISBN: 978-0-12-801942-9. DOI: https://doi.org/10.1016/B978-0-12-801942-9.00008-2. URL: http://www.sciencedirect.com/science/article/pii/B9780128019429000082.

[11] Donald W McRobbie Elizabeth A Moore and Martin J Graves. "MRI from Picture to Proton". In: *Cambridge university press* (2017).

[12] Gary D. Fullerton. "Magnetic Resonance Imaging Signal Concepts". In: *RadioGraphics* (1986).

[13] Cynthia Paschal and H. Morris. "K-Space in the Clinic". In: *Journal of magnetic resonance imaging : JMRI* 19 (Feb. 2004), pp. 145–59. DOI: 10.1002/jmri.10451.

[14] Fischl B van der Kouwe A Destrieux C Halgren E Segonne F Salat DH Busa E Seidman LJ Goldstein J Kennedy D Caviness V Makris N Rosen B Dale AM. "Automatically parcellating the human cerebral cortex". In: *Cereb Cortex* (2004).

[15] Fischl B Salat D van der Kouwe A Makris N Segonne F Quinn B Dale A. "Sequence-Independent Segmentation of Magnetic Resonance Images". In: *Neuroimage* (2004).

[16] A.M. Fischl Bruce Sereno M.I. Dale. "Cortical Surface-Based Analysis I: Segmentation and Surface Reconstruction". In: *NeuroImage* (1999).

[17] A. M. Fischl B.R. Sereno M.I. Dale. "Cortical Surface-Based Analysis II: Inflation, Flattening, and Surface-Based Coordinate System". In: *NeuroImage* (1999).

[18] Fischl Bruce and Dale A. "Measuring the Thickness of the Human Cerebral Cortex from Magnetic Resonance Images". In: *Proceedings of the National Academy of Sciences* (2000).

[19] Maks Ovsjanikov et al. "Functional Maps: A Flexible Representation of Maps between Shapes". In: *ACM Trans. Graph.* 31.4 (July 2012). ISSN: 0730-0301. DOI: 10.1145/2185520.2185526. URL: https://doi.org/10.1145/2185520.2185526.

[20] Simone Melzi et al. “Functional Maps for Brain Classification on Spectral Domain”. In: *Spectral and Shape Analysis in Medical Imaging*. Ed. by Martin Reuter, Christian Wachinger, and Hervé Lombaert. Cham: Springer International Publishing, 2016, pp. 25–36. ISBN: 978-3-319-51237-2.

[21] M. Aubry, U. Schlickewei, and D. Cremers. “The wave kernel signature: A quantum mechanical approach to shape analysis”. In: *2011 IEEE International Conference on Computer Vision Workshops (ICCV Workshops)*. 2011, pp. 1626–1633. DOI: 10.1109/ICCVW.2011.6130444. URL: https://ieeexplore.ieee.org/document/6130444.

[22] Jian Sun, Maks Ovsjanikov, and Leonidas Guibas. “A Concise and Provably Informative Multi-Scale Signature Based on Heat Diffusion”. In: *Computer Graphics Forum* 28.5 (2009), pp. 1383–1392. DOI: 10.1111/j.1467-8659.2009.01515.x. eprint: https://onlinelibrary.wiley.com/doi/pdf/10.1111/j.1467-8659.2009.01515.x. URL: https://onlinelibrary.wiley.com/doi/abs/10.1111/j.1467-8659.2009.01515.x.

[23] Paul J. Besl and Neil D. McKay. “Method for registration of 3-D shapes”. In: *Sensor Fusion IV: Control Paradigms and Data Structures*. Ed. by Paul S. Schenker. Vol. 1611. International Society for Optics and Photonics. SPIE, 1992, pp. 586–606. DOI: 10.1117/12.57955. URL: https://doi.org/10.1117/12.57955.

[24] John H. McDonald. *Handbooh of biological statistics*. 2nd ed. Vol. 1. Baltimore Maryland U.S.A.: Sparky House Publishing, 2009. ISBN: 1257140183.

[25] Henry B. Whitney Donald R. Mann. “On a Test of Whether one of Two Random Variables is Stochastically Larger than the Other”. In: *Annals of Mathematical Statistics* (1947).